EXPERIMENTAL AND COMPUTATONAL ANALYSIS ON THE EFFECT OF PCB LAYER COPPER THICKNESS AND PREPREG LAYER STIFFNESS ON SOLDER JOINT RELIABILITY

By

SANJAY MAHESAN REVATHI

Presented to the Faculty of the Graduate School of

The University of Texas at Arlington in Partial Fulfillment

Of the Requirements

For the Degree of

MASTER OF SCIENCE IN MECHANICAL ENGINEERING

THE UNIVERSITY OF TEXAS AT ARLINGTON

MAY 2015

ACKNOWLEDGEMENTS

Foremost, I would like to express my sincere gratitude to my advisor Prof. Dereje Agonafer for his continuous support for my master's study and research, for his patience, motivation, enthusiasm and immense knowledge. I would like to take this opportunity to thank him for giving me a chance to work at EMNSPC and for his continuous guidance during that time. It's been an excellent time working with him in research projects and an experience to learn so much from him. I also thank him for serving as the committee chairman.

I would like to extend special appreciation to Dr. A. Haji-sheikh and Dr. Kent Lawrence for serving on my committee and for providing numerous learning opportunities.

I would like to thank A. R. Nazmus Sakib, who was not only a PhD student but also a good mentor and a good friend who helped me throughout my thesis, providing new ideas and helping me learning new things. I would like to extend my special thanks to all mu lab colleagues for their constant support. Special thanks to Sally Thompson and Debi Barton for assisting me in almost everything. You all have been wonderful.

I would like to thank Alok Lohia for their expert inputs while working on the SRC funded project, which is a part of my thesis.

Last but not the least I would take this opportunity to thank my family and all my friends for their constant support and care. Without their support this would be possible

April14, 2015

ABSTRACT

EXPERIMENTAL AND COMPUTATIONAL ANALYSIS ON THE EFFECT OF PCB LAYER COPPER THICKNESS AND PREPREG LAYER STIFFNESS ON SOLDER JOINT RELIABILITY

SANJAY MAHESAN REVATHI, M.S

The University of Texas at Arlington, 2015

Supervising Professor: Dereje Agonafer

The emphasis of this study is to find out how the solder joints of the BGA package are affected with change in the stack up PCB layer copper thickness and the prepeg layer stiffness. In general the effect of the PCB layer thickness is to increase the stress and strain range and to decrease the thermal fatigue life. Basically a PCB consists of different layers with different material properties (Eg: Cu, FR4 etc.).In this paper we deal with the PCB with 1-6-1 configuration (6 core layers and 1 prepeg layer on the top and bottom). A Prepeg is a fiber glass impregnated with resin. The resin is pre-dried, but not hardened, so that when it is heated, it flows, sticks, and is completely immersed. The different layers with different material properties inside the PCB make the PCB highly orthotropic. Additionally, prepreg materials are visco-elastic and they provide some sort of stress relaxation and creep characteristics. Now when the PCB/package assembly is subjected to accelerated thermal cycling tests to assess the reliability, induced stresses are relaxed at a rate which is equivalent to the creep/stress relaxation rate.

The PCB is characterized experimentally. The CTE is calculated using the Digital Image Co relation (DIC) Technique and the young's modulus of elasticity of the PCB is determined from tension test using INSTRON micro Tester. A 3D model of the whole package is formulated in ANSYS 15.0 and static structural analysis is carried out to determine the accumulated volume

averaging plastic work. The fatigue co relation parameter is determined by using energy based and strain based models. The thickness of the Cu layers is increased and decreased by 50% and Prepreg layer stiffness in increased and decreased by 50% and the comparative study is done to predict the fatigue life of the package. The main purpose of the study is to understand the root cause for the solder joint failure and to obtain better methodology for a reliable design.

TABLE OF CONTENTS

LIST OF ILLUSTRATIONS

LIST OF TABLES

Chapter 1

INTRODUCTION AND OBJECTIVE

1.1 Introduction to electronic packaging

In this modern world the requirement of customer needs for consumer goods such as cellular phones, smart phones and smart watches has increased drastically which has increased the influence of electronic packaging in people's lives. The electronic packaging deals a major role in connecting the electronic components that make up an electronic product. The function of transmitting data generally takes place between a number of electronic devices called Integrated Circuits (ICs) Typically the integrated circuits are small wafer made or other semi conducting materials that are inter connected by different levels of electronic packaging.

The trend for microelectronics has historically been towards featuring smaller size, low cost, higher speed and high power. The current trend such as smart phones with a thin design challenges the packaging industry for increased IC performance characteristics and low size. The evolution of chip carrier designs reflects a trend towards smaller size and higher number of interconnects. The motivation behind these types of advances has traditionally been micro Processors. Due to the drastic growth in wireless communication, RF applications are the driving force for the microelectronics and traditionally led to the advancements in microprocessor. The packaging trend for these applications is driving to modulus that is simpler to integrate but on the other hand increases the complexity of the packages (i.e., multiple die, 3D packages, and passive devices into simple package).

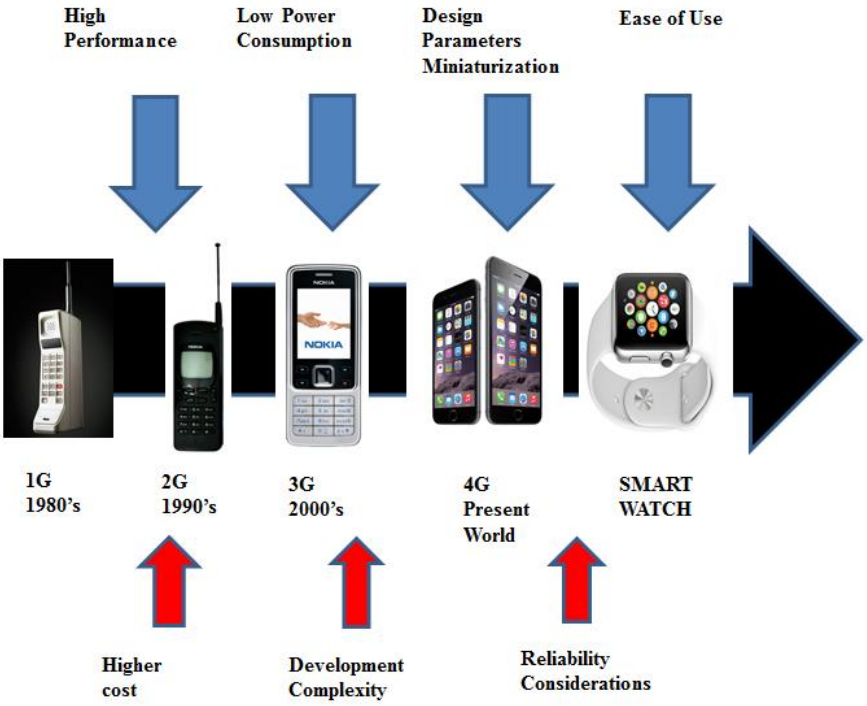

Figure 1.1 Evolution of Electronic Packaging

An electronic package integrates di electrics, semiconductors and metal conductors to form into a functional device. This variety of material inside a single package results in building into a complex system and increasingly retains high levels of reliability. Reliability is dependent on various factors like the operation of the device (power consumption. Heat dissipated) and the environment (ambient temperature, temperature changes, environmental strains). The differences in the co efficient of thermal expansion of the materials inside the package results in imposed strains, mismatch in temperature dependent properties and may propagate crack due to the temperature changes. Elevated operating temperatures may degrade/ change in the mechanical properties of the package and affect the reliability of the package. Additional to this Europeans Union's Waste in Electrical and Electronic Equipment (WEEE) and Restriction of Hazardous Substances (RoHS) Directives restrict the use of Lead in electronics. The Usage of lead free solder alloys not only

changes the solder built also affects other materials inside the package since there is a need of higher processing temperatures associated with the lead free solder alloys.

It is clear that the solder joint interconnects are very critical for the reliability of the package and hence it is utmost important to determine the factors that affect the solder joint reliability of the package.

1.1 Integrated Circuits

Integrated Circuit (IC) packages are what encapsulates the Die (Integrated Circuit) and splays it onto a device or component where we can easily connect to. An Integrated Circuit is also called as monolithic Integrated circuit which is an assembly of various components connected together to form one small semiconductor wafer (Silicon). An Integrated Circuit can basically function as an amplifier, oscillator, computer memory or microprocessor. A particular IC is categorized depending on intended application as either linear (analog) or Digital.

The IC package is distinguished based on the way they are mounted on the PCB. Packages are broadly classified as follows.

- Through Hole IC packages
- Surface Mount IC Packages
- Contactless Mount IC Packages.

The different types of IC packages based on the mounting style and the materials used for manufacturing are clearly pictured in the Fig 1.2 as shown below.

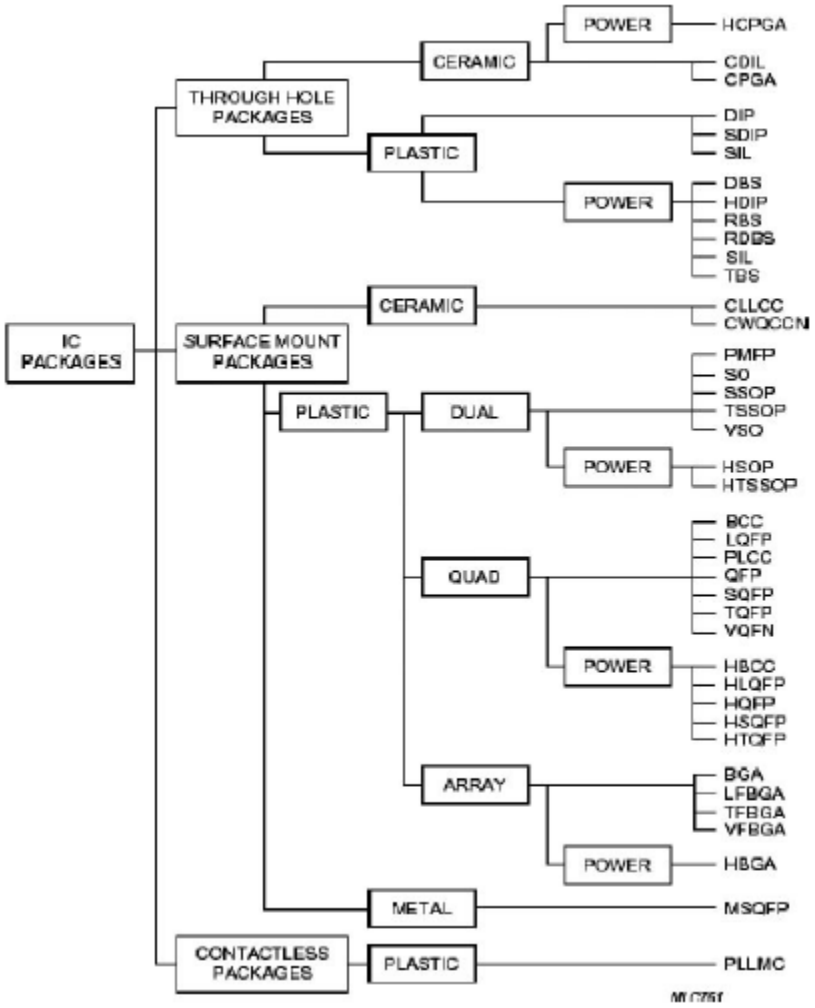

Figure 1.2 Different Types of IC packaging Techniques

1.2 Ball Grid Array (BGA) Packages

A Ball Grid array or BGA package is one of the product surface mount Technology or SMT package that is being used drastically for Integrated circuits. The Ball Grid Array package was designed to have a convenient package for Integrated circuits and to have a robust design with large number of interconnects.

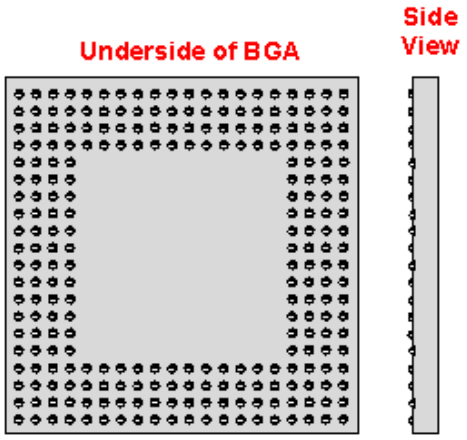

Figure 1.3 Schematic of a Ball Grid Array Package

The Ball Grid Array (BGA) package uses a different kind of approach i.e., conventional surface mount connections whereas the quad flat pack used the sides of the package to connect to the PCB. The BGA package uses underside of the package where there is a considerable area of connections. The BGA package uses solder balls or bumps for connectivity and are placed in a grid (Hence the name Ball Grid Array) on the under surface of the chip carrier. Apart from the improved connectivity, the BGA package has other advantages such as lower thermal resistance between the silicon chip compared to the QFN packages.

1.1.1 Types of BGA Packages.

Based on the material used and connectivity and other features, the BGA package is classifies into 5 types.

- MAPBGA – Molded Array Process Ball Grid Array
- PBGA – Plastic Ball Grid Array
- TEPBGA – Thermally Enhanced Plastic Ball Grid Array
- TBGA – Tape Ball Grid Array
- MicroBGA

1.2 Objective

1.2.1 Motivation

An Enormous growth in the research and development for Ball Grid Array Packages (BGA) has been going on in the past few years. Over the last 2 to 3 years, standard area array packages have become the package of choice for both design and manufacturing. This technology has very good advantages over the traditional leaded packages for many reasons such as increased I/O per unit area of the PCB, higher capability and functionality, good performance and higher production yields. Apart from these todays customers' needs include Demand for smaller products, Very high power and increase performance characteristics and very good reliability. Because of the demands identified, BGA packages are becoming more into picture and flip chip applications that are being enhanced.

As stated by John H. Lau et, al [3] the effect of the buildup layer of PCB on the solder joint reliability is to increase the stress range, creep strain range, and creep strain energy density range in the solder joints and to reduce the thermal fatigue life. Significant differences between the properties within package and also between layers of PCB cause extensive internal stresses. Once the package is mounted onto the PCB, the solder joint must absorb all the strains induced by the expansion of the package and also by the PCB in thermal excursions. In area array devices, such as in ball grid arrays (BGA), the joint alone must provide CTE mismatch compliance. The board thickness and over all stiffness decrease will decrease the stress distribution in the solder joint is stated by Anthony. A. Primavera in [4]. Due to high stiffness inside the PCB layers compared to the package and due to the CTE mismatch between the PCB and package might have a high probability of the solder joint failure at high temperatures.

Two 11x11 pin Micro star BGA package of thickness 1 mm each with different Prepreg materials are tested under accelerated thermal cycling (ATC) conditions for Failure Analysis. The two prepregs used are FR4 material as one and other Resin Coated Copper (RCC) are used for two different PCB. The boards were tested for the temperature loading from -40ºC to +125ºC. With a 20 min dwell time. The test showed that the boards failed at 571 cycles and 577 cycles.

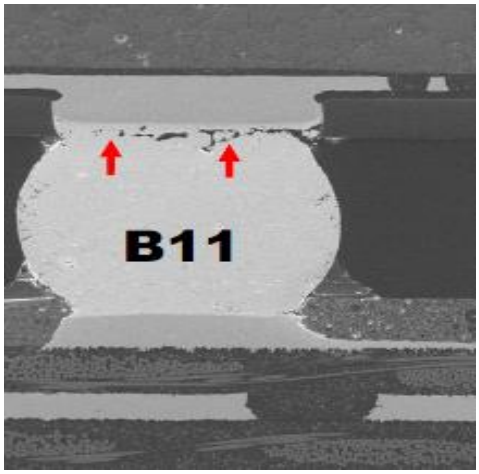

Figure 1.4 Failure Occurred on the Substrate Side of the Package

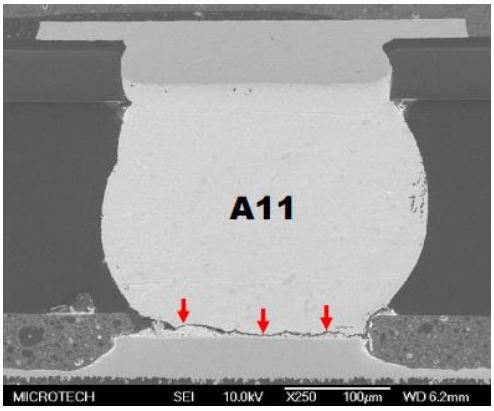

Figure 1.5 Solder Joint Failure occurred on the PCB side

From the test Results of the two BGA packages, we have observed that the solder joint is failing on both sides (i.e., top and bottom). Since the Prepreg layers are varying and the failures is different for different boards creates the motivation for this work. The work included covers how the Prepreg layer stiffness affects the solder joint reliability of the BGA package. Also the copper thicknesses are also varied to predict the reliability by increasing and decreasing the thicknesses.

1.2.2 Goals and Objective

The Primary objective of this work is to determine the root cause for the failure in the solder joints in the BGA package and methods to improve the mechanical reliability of the package and to meet customer requirements. Finite Element Analysis (FEA) is used to determine the fatigue co relation parameters such as strain energy density, plastic strain range, and accumulated volume average plastic work to predict the characteristic life of the package. Various strain based and energy based models are used to predict the fatigue life. The comparative study is done for the cases with the stiffness of the prepreg layer increased and decreased by 50% and also with the copper thickness increased and decreased by 50% and the life is predicted. The best case for good robust and reliable design is proposed

Chapter 2

LITERATURE REVIEW

Anthony A. Primavera [4] discussed some of the basic assembly and PCB parameters that affect the success of CSP assembly and solder joint robustness. The long term solder joint reliability of CSP package has been assessed using the accelerated thermal cycling and various mechanical test methods. Using the Finite element modelling the reliability modelling is done to compare the predicted fatigue life test data from both 0-100^{o}C and -40 to 125^{o}C thermal cycles. It has been stated that when the board thickness and overall stiffness decreases, the stress on the critical solder joint in the CSP package decreases and has a 2X increase in the fatigue life. It has been said that the effective CTE of the device is reduced; the expected life of the solder joints is reduced.

John. H. Lau., et al [3] has done the creep analysis of a solder bumped wafer level chip scale package on a Printed circuit board (PCB) with microvia subjected to thermal cycling. It has been stated that due to the large co efficient of thermal expansion of the buildup resin, the effect of the thickness of the PCB with microvia build up layer become much more significant than without the microvia buildup layer. The Shear stress and creep shear strain hysteresis loops, shear stress range and creep shear strain range , creep strain energy density range at different locations in the critical solder is studied for better understanding of the thermal-mechanical reliability of a WLCSP on a Printed circuit board.

Biju Chandran et. al., [5] has done the finite element analysis and physical failure analysis on a typical BGA package to determine the effect of design features like the Grid pattern, Package size on the propensity of the fatigue failure. It has been concluded that the risk to fatigue failure was much greater on partial BGA than a full grid array package. The parameters and variables affecting the solder joint of BGA were determined to be the die size and the temperature conditions.

The PCB length and width dimensions in the model have significant effect on the solder joint behavior at the package corner, but not on the solder joints under the die shadow region was

stated by Pradeep K. Bhatti et, al., [6]. The mechanical test setup and experimental data are used to evaluate the reliability of the solder joints and a nonlinear finite element analysis is performed to simulate the effect of compressive load in thermal cycling. It has been stated that a more advanced fatigue law formulation is need to correctly predict the failure location and the fatigue life of solder joints.

Chapter 3

TENSILE TESTING

3.1 Introduction

The tensile testing also known as Tension Test, is one of the most fundamental mechanical test performed to determine the behaviors of the body subjected to tensile force. Tensile Tests are performed for several reasons. The results obtained from the stress strain graph are used in selecting the materials for engineering applications. The tensile properties of a material basically ensure the quality and strength of the material we used in certain applications. Tensile properties often are determined during the development of new materials, so that the different material properties of different materials and processes can be compared. Properties that are measured from tensile testing include ultimate tensile strength, maximum elongation and area reduction. Young's modulus of elasticity, Poisson's ratio, yield strength, strain hardening characteristics can be determined from the above measurements.

3.1.1 Hooke's Law

Robert Hooke in 1676 stated that "Extension is directly proportional to the Load" which explains that for relatively small deformations of an object, the displacement or size of the deformation is directly proportional to the deforming load. The object tends to return to the normal position after the applied load is removed under these conditions. Elastic behaviors according to the Hooke's law can be explained that small displacements of their constituent molecules, atoms caused due to the tensile load is proportional to the load that causes displacement.

$$F_{Load} = -kx$$

Where f = Load applied

K = Proportionality constant or spring constant

X = Displaced due to the load

3.1.2 Stress Strain Curve

As the axial loading is gradually increased at certain elongation rate, the total elongation over the gauge length is measured at certain increment of the load is measures until the specimen experiences failure. The cross section of the specimen and the initial length of the specimen are known and the normal stress and strain can be calculated. The graph with stress along the vertical axis and Normal strain on the horizontal axis is plotted to get the stress strain curve as shown in the figure 3.1.

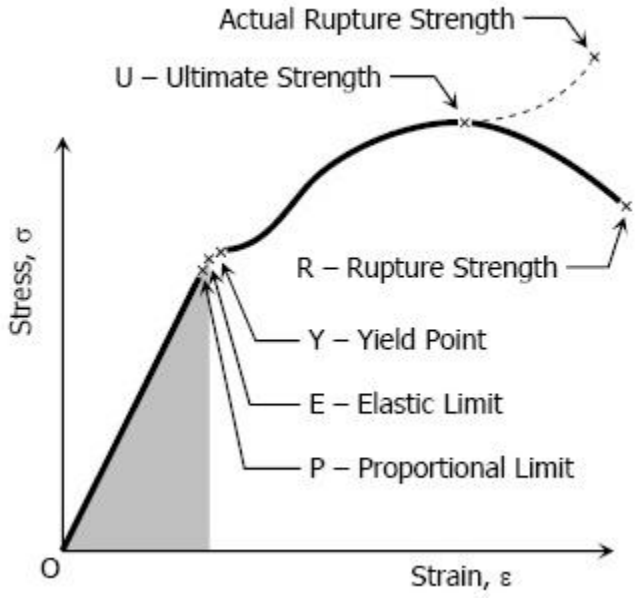

Figure 3.1 Stress – Strain Curve

Metallic engineering materials are classified into ductile or brittle materials. Ductile materials have higher strain range compared to the brittle materials. Different portions of the stress strain graph contribute certain limits such as

- Proportionality Limit (Hooke's Law)
- Elastic Limit
- Yield Point

- Ultimate Strength
- Rupture strength
- Modulus of Resilience
- Modulus of Toughness

3.2 Test Methodology

This section explains the steps involved during the tensile testing of the PCB. The mail steps include

- Selection of the sample
- Dog Bone specimen Preparation
- Test Setup
- Test Procedure
- Data Recording
- Data Analysis

3.2.1 Selection Of the sample.

The basic objective during material testing is to determine whether the sample is suitable for the intended use or not. There are many considerations for a good test such as uniform cross section of the specimen, grain patterns near the critical parts of the specimen. Since the tensile test done here is on the PCB and since the populated boards are used it is surely important that the

specimen we select is free from holes, grooves and other texture patterns. The results that we obtain with the samples with irregularity in the cross section may give bad results.

Figure 3.2 Dog Bone Specimen made out of PCB

3.2.2 Dog Bone Preparation

Dog bone samples are basically used for the tensile tests. The sample has a gauge section in between and a shoulder at each ends. The shoulder is wider than the gauge section also known as the grip section. The shoulder wider than the grip section causes a stress concentration to occur in the middle of the specimen when the tensile loading is applied. The stress concentration in the middle of the specimen ensures the specimen to rupture away equally from both the ends if not the

sample may rupture at one end or near the grip section itself. Basically the dog bone specimen ensures that the loading applied tends the stress to be concentrated at the middle of the specimen and to ensure the highest probability that the sample fails at maximum tensile loading.

There are several methods that can be used to create a dog bone sample. Most commonly used methods are cutting and molding. The method used for creating the dog bone specimen out of a PCB is cutting. ASTM standards are used for preparing the dog bone sample. The dimensions are scaled up and down depending on the maximum width of the specimen. The corner part of the PCB board is used for preparing the Dog bone specimen as shown in the figure 3.3

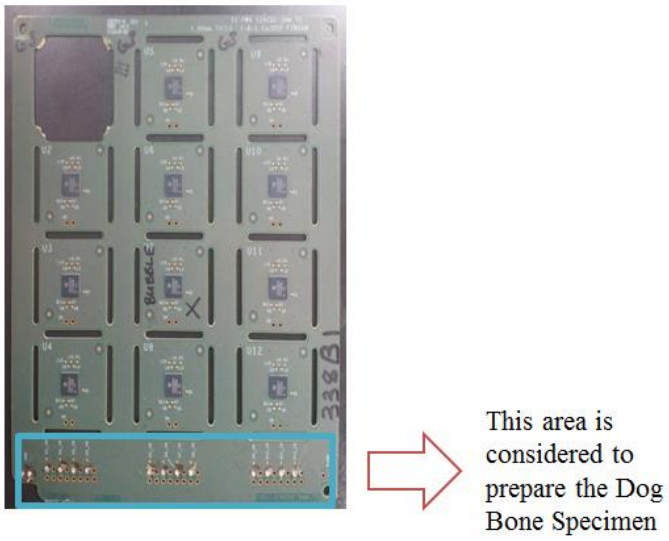

Figure 3.3 Portion of PCB considered for Dog Bone Specimen Preparation

To cut the sample out of the PCB a cutting machine is used to cut a rectangular portion from it. The Gauge length, grip section the radius of curvature are determined from the scaled

down ASTM standards chart. Milling technique is used to obtain the curved surface near the shoulder as shown in the fig 3.2.

3.2.3 Test Setup

The test setup requires that the equipment be properly matched for the test by hand. Basically there are three requirements for the Tensile testing machine as listed below.

- Force capacity sufficient for the breaking point to occur during the test.
- Loading rate (Strain Rate)
- Precision sufficient to obtain the data generated by the test. (Ensured by calibration certification).
- Proper selection of grips.

There are many types of grips that are used for tensile testing. Suitable grip that properly fix the specimen and also which avoids slippage is used. The grips used must be capable enough to handle the applied tensile force so that they are not damages during the testing.

Various potential problems must be taken into considerations during the test setup including the specimen misalignment. The alignment of the specimen at both the points are important, because any off center loading will cause the specimen to undergo bending. This problem is more while tensile testing a brittle material and also for ductile materials. Misalignment also may lead to load-measurement errors due to effect of bending forces through the load measuring apparatus.

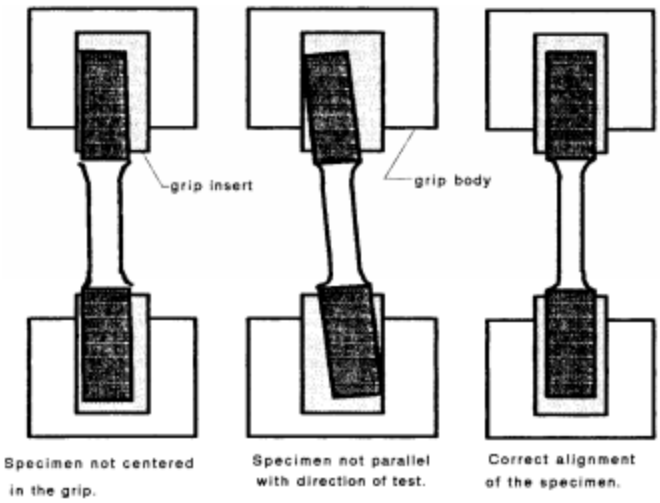

Figure 3.4 Improper alignment of the Specimen

Basically tensile tests deals with the strain measurements. Strains are commonly measured using extensometers, strain gauges etc. Here in this test we use extensometer to determine the strain at particular loading conditions. In order to obtain the accurate strain values, the extensometer is to be installed properly. The extensometer must be calibrated, i.e, setting the extensometer gage length to zero. The extensometer reading must be set to zero repeatedly before and after the test in order to maintain the accuracy.

3.2.4 Test Procedure

3.2.4.1Blue Hill Software Setup

- Turn on the tensile testing machine. Turn on the two control system units.
- Go to the desktop and launch the Blue hill Software.
- On main page select Test to start a new test. Name the test and select the destination folder for the output file.
- Choose the method or create the new method by giving the maximum loading and elongation rate.

3.2.4.2 Instrument Setup

Instron Micro tester is used for the Determining the Young's modulus of elasticity of the PCB. The instrument setup is shown in the Fig 3.5

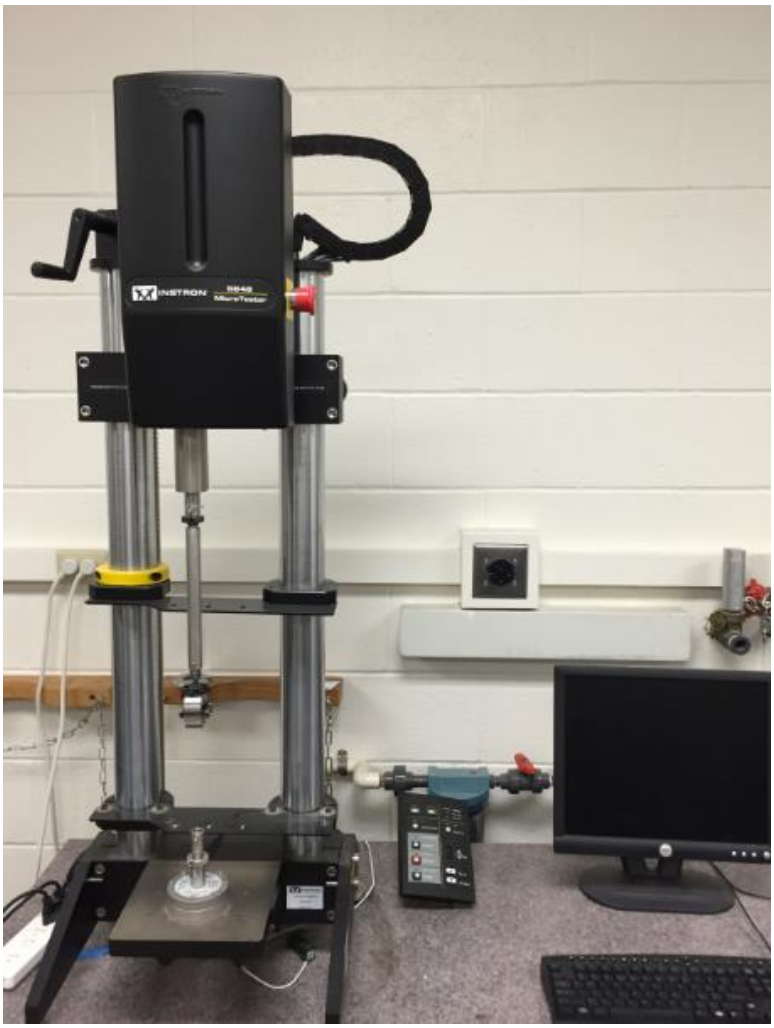

Figure 3.5 Instron Tensile Testing Machine

Proper precautions and standardized steps are performed to obtain the accurate results and for the individuals safety. ASM Test procedure standards are used to perform the experiment. The detailed procedure are discussed below.

- Make sure that proper load cell is installed, 2Kn, 10Kn 50KN depending on the load range and the material we are testing.
- Calibrate the load cell by clicking the upper right button on the blue hill software. Make sure all loads are removed and click calibrate to calibrate the load cell.
- Install the clamps/Jaw faces for testing depending on the width of the dog bone specimen. Zero the loads after the jaw faces are installed.
- Use the remote to Jog up/down the clamps depending on the length of the dog bone specimen, gauge length.
- Adjust the Jaw face so that the $3/4^{th}$ of the grip section of the dog bone specimen is inside the clamp and affix the clamps and make sure that there is no slippage while the application of load.
- Make sure that the specimen is aligned accordingly without and torsional forces acting rather than axial force.
- Fix the extensometer on to the gauge length of the specimen as shown in the Fig 3.6 and calibrate the extensometer to zero.
- Make sure all the steps are performed correctly and start the test.

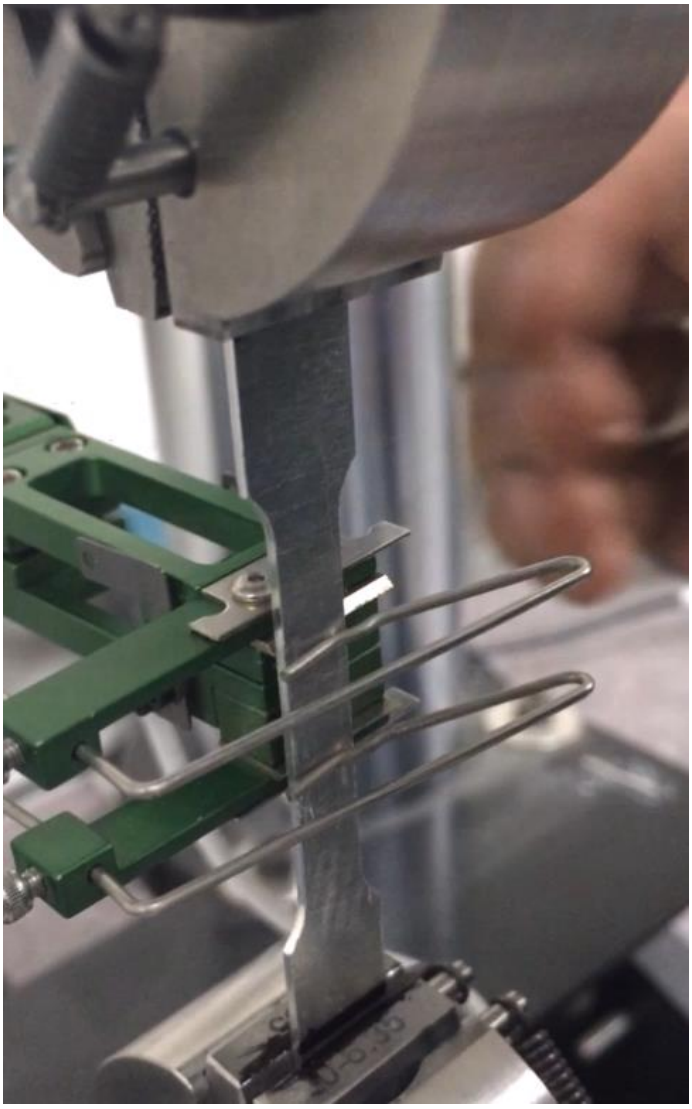

Figure 3.6 Placement of extensometer

3.3 Results and Discussion

The results of the tensile testing is used to determine how the material under loading conditions behave and also to determine the Young's modulus of elasticity. It is desirable to plot the data in terms of true strain and true stress. From the extensometer installed the strain at certain loading intervals is recorded.

True stress σ is defined as

$$\sigma = F/A$$

Where F is the applied force

A is the cross sectional area of the specimen

True strain ε s defined as

$$\varepsilon = \ln (L/Lo)$$

Where L is the Change in length

Lo is the original length

True strain definition in nothing but the incremental change in the length to the original length. As long as the deformation under the tensile loading is uniform, the true strain can be calculated mathematically. Here in this experiment the true strain is calculated from the Extensometer readings.

The strain is directly recorded from the extensometer and the stress is calculated mathematically from the load applied to the cross section of the specimen used. A graph is plotted with stress on X axis and strain on Y axis as shown in the figure 3.7 and figure 3.8. The slope is calculated to get the young's modulus of the material.

The Tensile tests are performed for both the boards with RCC and FR4 Prepreg and the results are discussed. The young's modulus calculated is found out to be 28.5 GPa for the PCB with FR4 prepreg layer and 27.8 GPa for the PCB with RCC prepreg Layer.

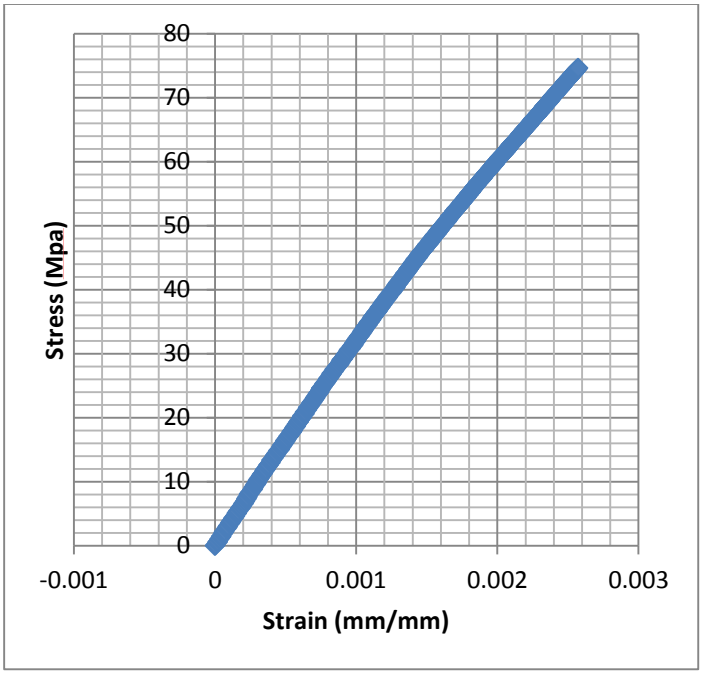

Figure 3.7 Young's Modulus FR4 Prepreg

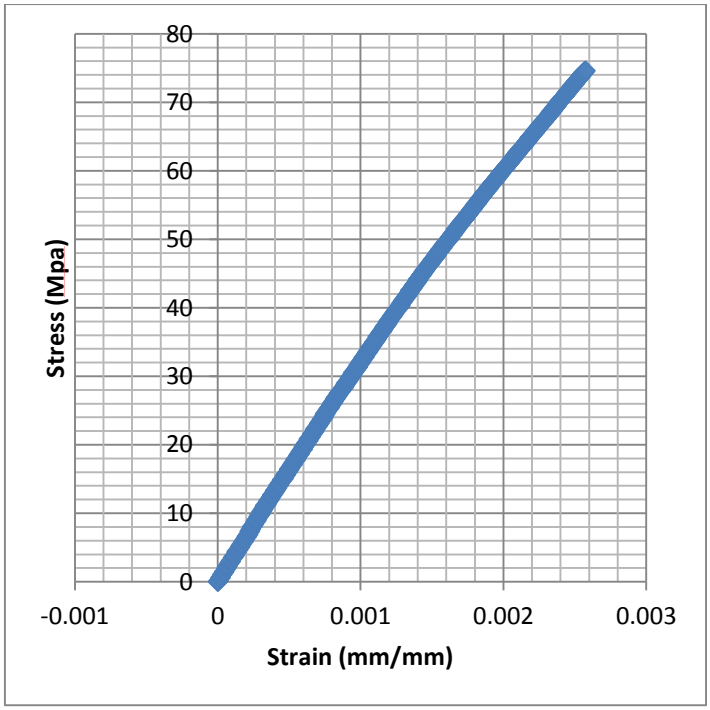

Figure 3.8 Young's Modulus RCC Prepreg

Chapter 4

DIGITAL IMAGE CORRELATION TECHNIQUE

4.1 Introduction

Digital Image Correlation technique is a full field in plane and out of plane image analysis method, that determine the contour and displacements of an object under mechanical or thermal loading using a high resolution digital images. This technique is often used to measure the deformation, strain, displacement and optical flow.

The non-contacting optical technique (Digital Image Correlation Technique) was been developed by sutton et al. (1983, 1986, 1988, 1991) and Bruck et al, (1989) The basic application of this technique was used to determine the displacement and strains in electronic packing field and strain fields in polyurethane foam plastic materials for evaluating the material properties of the materials and also to evaluate the thermal strains in the solder joints. This vision technique has the advantage of a simple system where we can obtain the results without disturbing the object under loading (Non-contact Setup) thus avoiding the interpretation and interferometric fringes. The basic principle of the technique is it uses the two speckle images, which are captured by high resolution, high frame per second capability digital video camera to compare the status of the object to detect the deformation before and after the application of the force. By utilizing the concept of digitalization we can characterize the image by different levels of patterns depending on the intensity of the light and the placement of the camera and also the capability of the cameras used. Both the digital images cameras are correlated by an algorithm, based on their mutual correlation coefficient or other functions to establish a relation between the two images.

The basic objective of the Digital image correlation technique depends on the ability to recognize two different images with same speckle pattern and correlate them using an algorithm to detect any changes in deformation or strain at the order of microns. The Newton -Raphson method can be used to determine the convergence in searching the local minimum with high accuracy.

4.2 Mathematical Principle of the Method

The basic principle of this technique was previously developed by M. A. Sutton et al. The image of an object can be represented by discrete function as a value between 0 and 255of its grey levels. The Correlation is basically done for a pattern. A pattern is nothing but a group of pixels. The initial image before distortion may be represented by the function f(x,y) after application of direct or indirect load may to transformed to another discrete function , let's say f*(x*,y*)[20]. The theoretical relation between these two discrete functions can be written as follows.

$$f^*(x^*,y^*) - f(x + u(x,y), y + v(x,y)) = 0$$

Where u(x,y) and v(x,y) represent the displacement field for the pattern. The pictorial representation of the displaced object is shown in figure 4.1

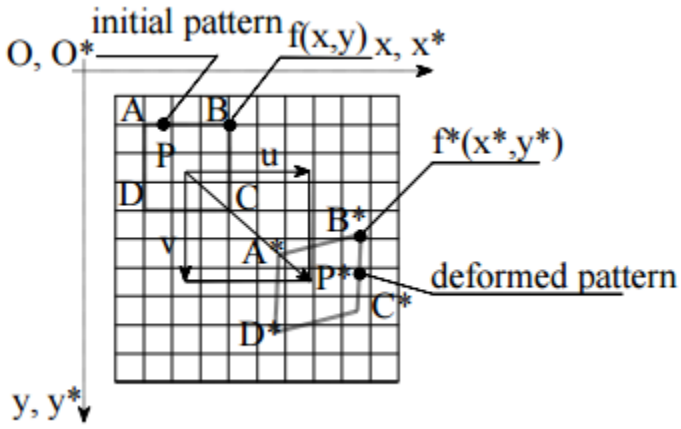

Figure 4.1 Initial and Deformed image represented in the same axes

The factors that explains the principle behind the digital image correlation technique are as follows

- Mathematical definition for the displacement field for a pattern which has t include the same time, strain terms and rigid body displacement.
- The mathematical correlation between the two functions f(x,y) and f*(x*,y*).

- Interpolation method for particular grey levels of the image to reach the précised sub pixel.
- Mathematical algorithm to determine the displacement and strain for a particular pattern.

Many parameters are responsible to get accurate DIC results that include the speckle size, speckle density, type of algorithm, grey level interpolation , subset size etc.,. The analysis procedure of the DIC is shown in the fig 4.2. The analysis is divided into several sub steps. To identify the relative positions of the same point of an object is determined by the grey scale distribution. Correlation analysis of the images is carried out to determine the highest grey scale point co relating with the initial position displacement vector.

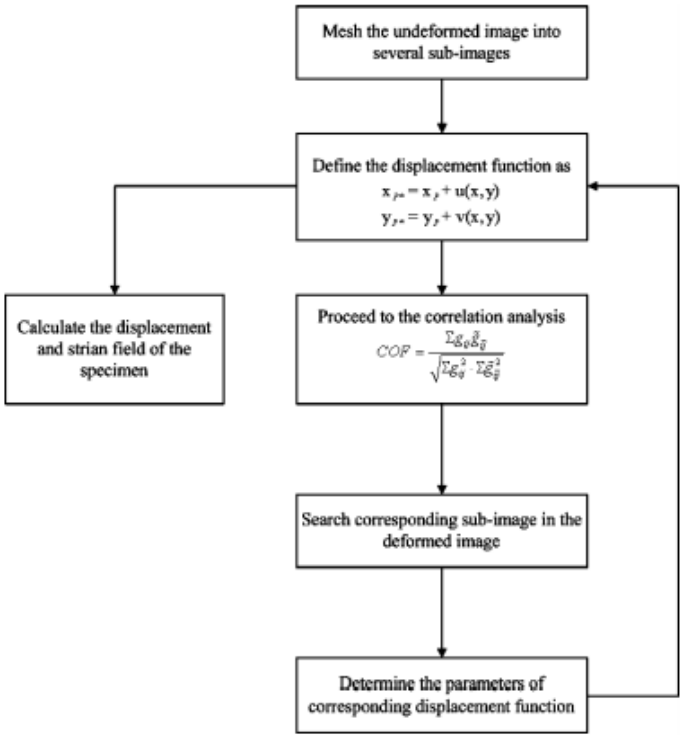

Figure 4.2 Analysis Procedure of DIC method

Consider a point P (x_p,y_p) and Q(x_q,y_q) on the same object initially in a position as shown in the figure 4.3 . On application of external loading the position of the same point has been displaced to the point P*(x_{p*},y_{p*}) and Q*(x_{q*},y_{q*}). The Functional correlation is expressed as follows.

$$x_{p*} = x_p + u(x,y)$$

$$y_{p*} = y_p + v(x,y)$$

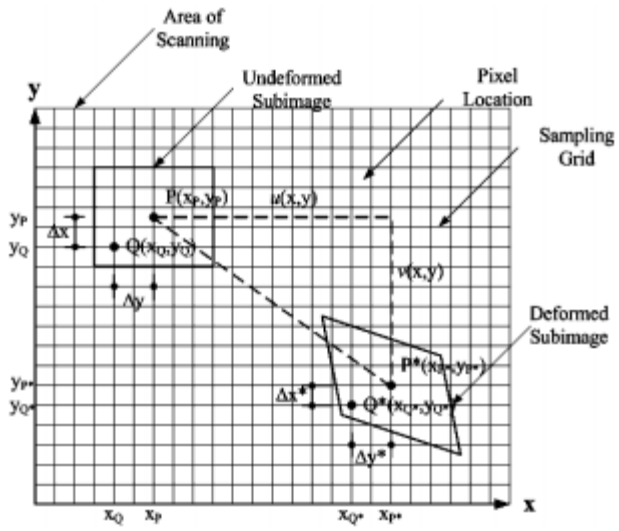

Figure 4.3 Correlation between deformed and non-deformed images.

Calculating the grey scale correlation coefficient will explain the relation between the deformed and non-deformed sub image. The Correlation coefficient is given by shis-Heng Tung et al. [6]. As follows.

$$COF = \frac{\sum gij.Gij}{\sqrt{\sum(gij)^2.\sum(Gij)^2}}$$

Where g_{ij} and G_{ij} are the grey scale of the non-deformed and deformed images on the coordinates (i,j) respectively.

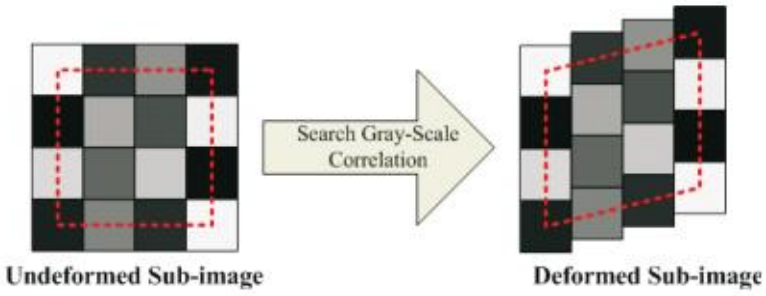

Figure 4.4 Grey Scale Correlation between deformed and non-deformed image

4.3 Experimental Setup

To start off the experiment few considerations must be taken care of. The experimental setup main involves

- Setting up the DIC
- Calibration of the DIC
- Specimen Preparation
- Setting up the oven with Thermocouple
- Results and Analysis

4.3.1 Setting up the DIC Equipment

The DIC equipment consists of 2 High speed High resolution high sensitivity cameras placed on a tripod with 9 degrees of freedom. The cameras are placed in a condition such a way that both the cameras are focused at a single point. Since in this experiment the Digital image correlation is used to determine the co efficient of thermal expansion, the specimen is place inside an Oven and non-contact technique is used to determine the CTE of the material. In such case the cameras are

placed outside the oven with the clear accessibility for the cameras to have a clear picture of the specimen to record the deformation of the specimen at particular temperature change. The cameras are placed in such a way that the specimen lies inside the focal length of the camera depending on the specification of the camera such as the resolution, No of pixels and frames per second captured. A detailed experimental setup is shown in the figure 4.5.

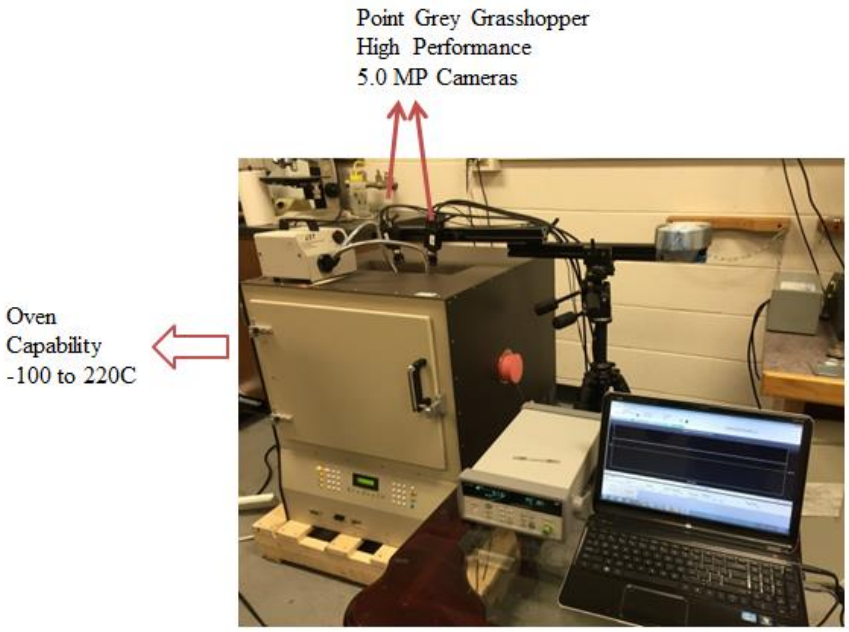

Figure 4.5 DIC Experimental Setup

The cameras used in the experiment are the Point Grey Grasshopper 3 series 5.0 MP Performance cameras. The cameras used are basically a 14 bit imaging cameras designed for the vision applications such as gauging, inspection and image correlation techniques. The cameras are

capable of capturing a 1928x1448 pixel images with a transfer speed of 5GB/Sec and 128MB frame buffer and electronic shutter speed ranging from 0.03-30 Sec.

To record the précised data and to capture the images without any errors, borosilicate glass is used over the oven through which the DIC cameras capture the specimen images. This precaution is taken since the oven heats up to 220^{o}C which should not affect the glass which eventually leads in recording and capturing error images. Borosilicate glass is basically known for low coefficient of thermal expansion which makes them resistant from thermal shock.

4.3.2 Calibration

Calibration is a set of operations under specified condition which establishes a relationship between the values indicated by a measuring system and the corresponding values realized by a reference model. Calibration permits the estimation of errors and indicates the measuring instrument. The calibration is most important before stating off the experiment because if is important to ensure that both the cameras are focused at a single point without any displacement in the focal length of the camera.

Here in this experiment a 12X9 and 4mm pitch calibration block is used to calibrate the Digital image Correlation system as shown in Fig4.6. It is not mandatory to use this pattern of calibration block; depending on how much area the cameras can cover the calibration grid can be generated by a Grid generator. It can be printed on a block or a paper to calibrate the system. The calibration can be easily done by capturing images of calibration block under different perspectives. The images about 35-50 are captured and is called with VIC 3D software for calibration. The bundle adjustment algorithm calculates the intrinsic parameters such as focal length, Principal point and distortion parameter and extrinsic parameters such as translation vector and rotation matrix for each camera from their respective orientation.

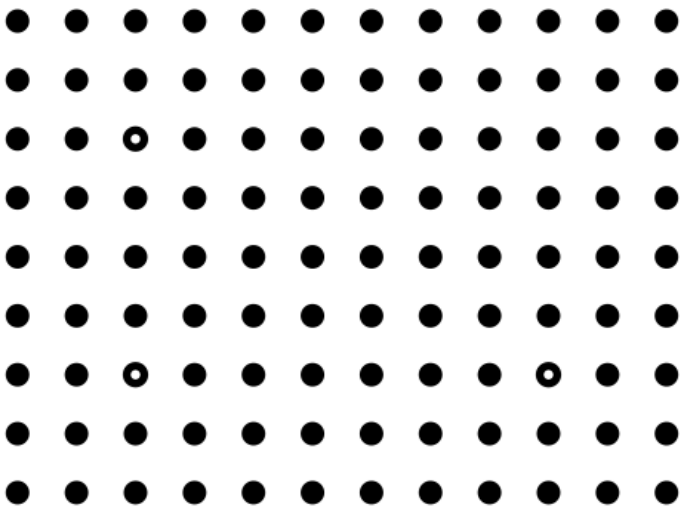

Figure 4.6 Calibration Grid Used for calibration

4.3.3 Sample Preparation

For précised strain measurements with from the digital image correlation technique it is mandatory to spray the specimen with appropriate speckle pattern. The speckle pattern can be obtained from various methods depending on the application and the size of the specimen. Here in this experiment an internal mix Aztek A 320 airbrush is used to paint the speckle pattern. The pattern is obtained from the black and white paint. Initially the specimen is sprayed with a white paint and left to dry for couple of hours. After a layer of white paint is sprayed, a black mist of spray is used to create the speckle pattern. To get a good pattern it is essential to maintain a 2 feet distance from the specimen and 20PSI pressure can be used to spray the optimum speckle pattern. The speckle pattern is selected depending on the relation between the pixel size and the camera resolution and the distance of the cameras from the specimen. A sprayed specimen is shown in the figure 4.7.

Figure 4.7 Specimen used for measuring the CTE

4.3.4 Setting up the Oven

To measure the Coefficient of thermal expansion it is necessary that the specimen has to be heated up or cooled down depending on the purpose to calculate strain at different temperatures.

EC127 Refrigeration chamber is used for heating and cooling down the specimen. EC127 temperature chamber is a closed loop, temperature controlled test chamber with an operating temperature from -30C to 200C. This refrigeration chamber is used to provide a wide temperature test range, stand-alone product assurance and reliability testing. The Refrigeration chamber is cooled by its single stage compressor system and used zero voltage controlled resistance heaters foe heating the chamber. The temperature chamber is also equipped with advance controller which provides precise temperature increase rate and maximum temperature set point.

Before starting the experiment the refrigeration chamber is equipped with a dummy sample and the thermocouple is placed over the dummy sample to ensure that there is no temperature difference between the specimen lower and upper surfaces. It is mandatory to maintain Zero ΔT between the layers of the specimen (PCB). A schematic showing the thermocouple placed on the dummy specimen is shown in the Figure 4.8.

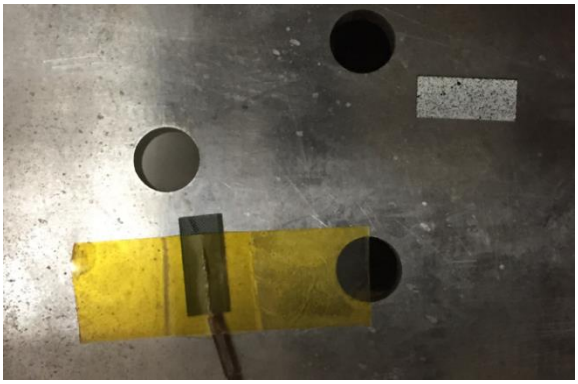

Figure 4.8 Thermocouple placed on the dummy specimen

4.4 Results and Analysis

The Maximum temperature used for measuring the Coefficient of thermal expansion is 125^{o}C starting off from the room temperature i.e., 25^{o}C. The Images are captured at regular intervals like at 25^{o}C, 50^{o}C, 75^{o}C, 100^{o}C and 125^{o}C using the Digital image correlation setup. The images captured are called using the software VIC3D for the evaluation of strain at different temperatures.

The strain at two different temperatures are considered to calculate the Coefficient of thermal expansion. The Coefficient of thermal expansion describes how the body dimensions changes with increase or decrease in temperatures. It is the measure of the fractional change in size per degree change in the temperature.

$$\frac{\Delta L}{L} = \alpha \, \Delta T$$

Where ΔL is the change in Dimension (Length)

L is the original Length

α is the Coefficient of Thermal Expansion

ΔT is the Change in the temperature

The Graph between the strain and the Temperature difference is plotted. The slope is calculated to determine the CTE of the PCB both in X and Y direction as shown in the Fig 4.9 and Fig 4.10.

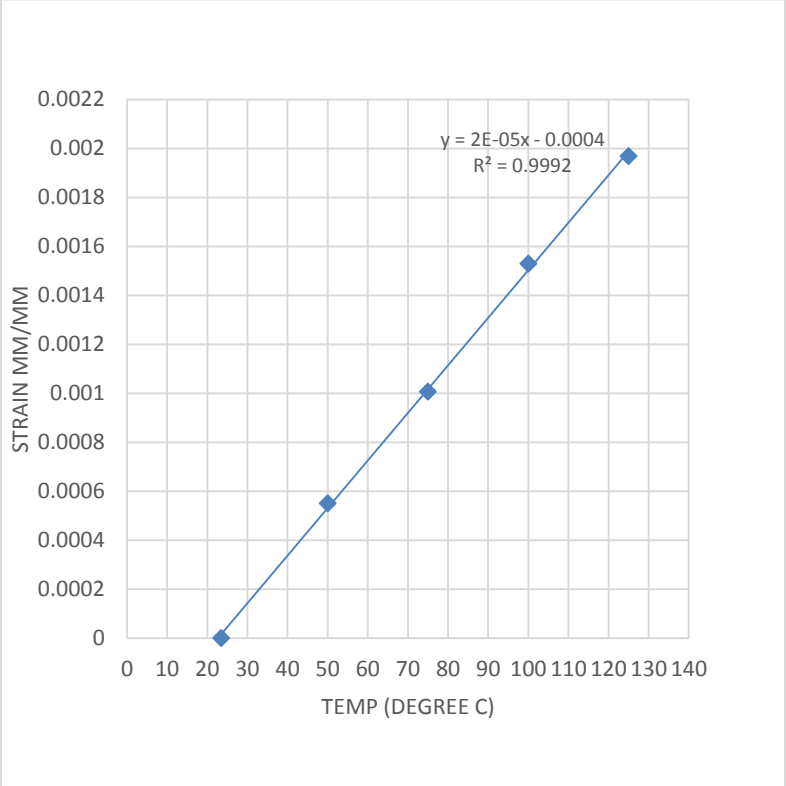

Figure 4.9 Coefficient of thermal expansion in X Direction

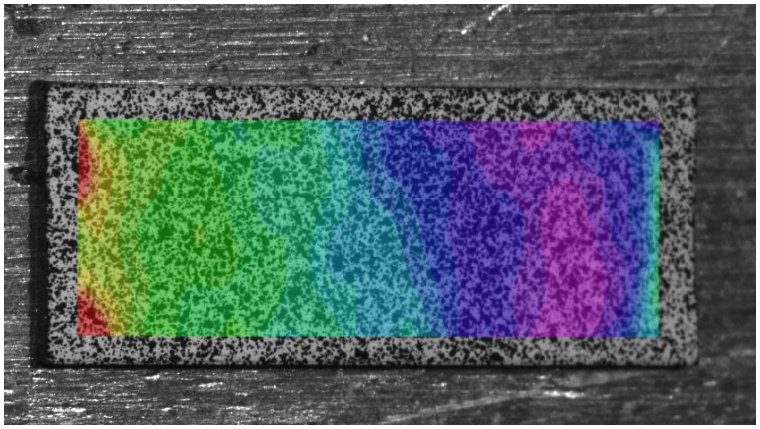

Figure 4.10 2D Contour of the strain in X Direction

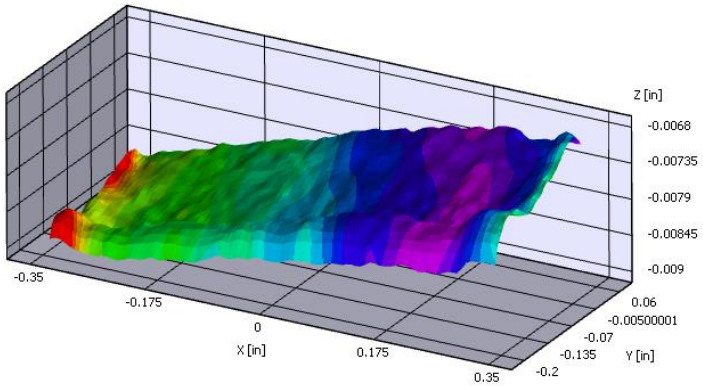

Figure 4.11 3D Contour of the strain in X Direction

Calculated Coefficient of Thermal Expansion in X direction = 19ppm/^{o}C

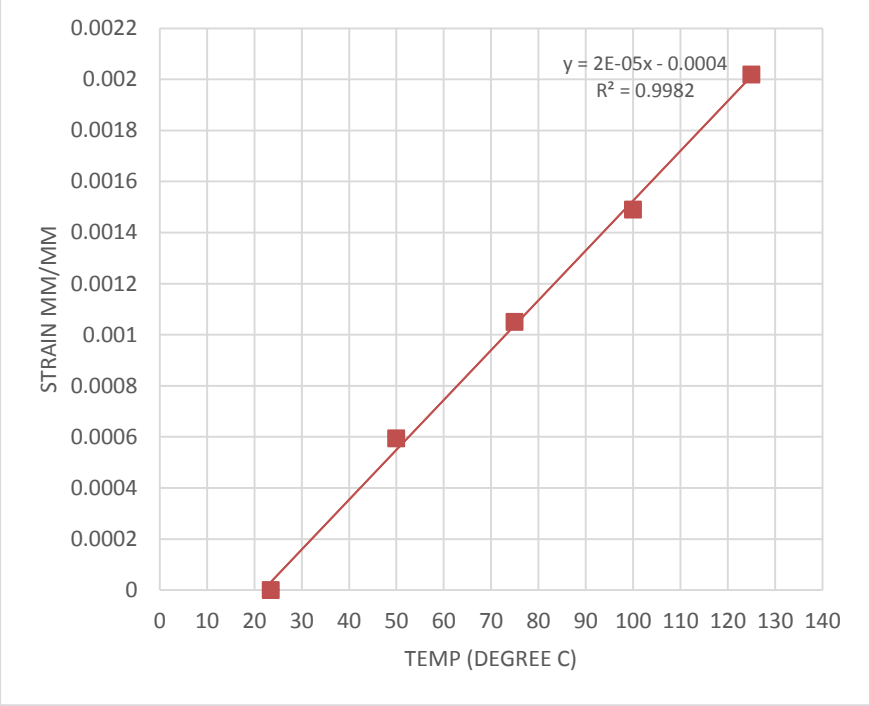

Figure 4.12 Coefficient of thermal expansion in Y Direction

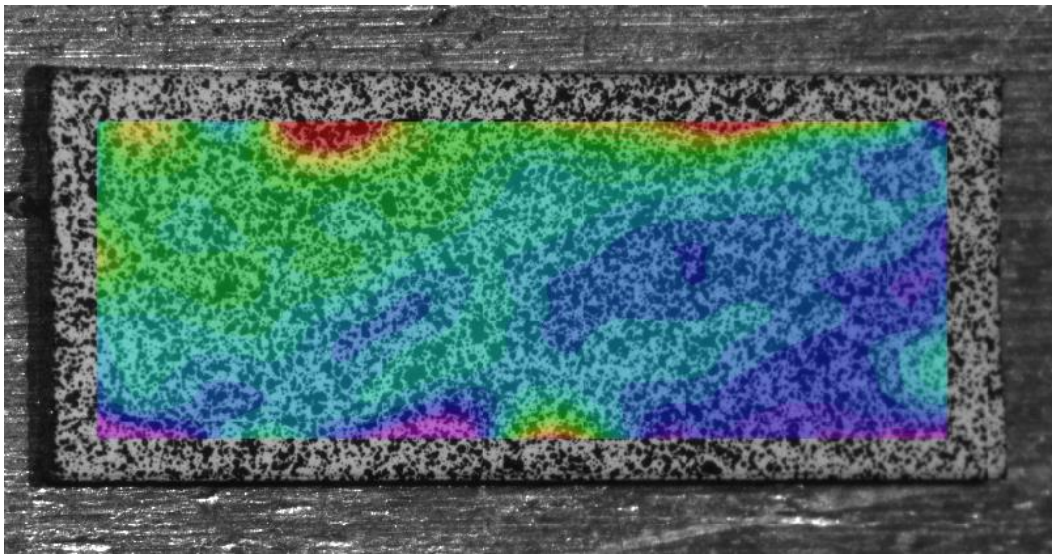

Figure 4.13 2D Contour of strain in Y Direction

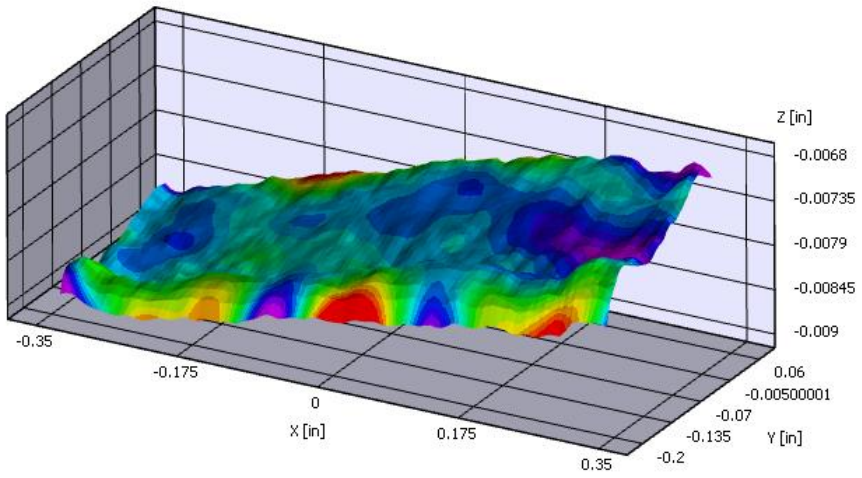

Figure 4.14 3D Contour of strain in Y Direction

Calculated Coefficient of Thermal Expansion in Y direction = 19.2ppm/ ^{o}C

Chapter 5

FINITE ELEMENT MODELING

5.1 Introduction

Finite element method/analysis is one of the computational technique used to get a solution out of a problem with defined boundary values. FEA is used in majority of the industries for various structural, thermal and vibrational analysis. Below listed are the applications of the Finite Element Analysis.

- Structural Analysis (Linear, Non Linear, Static, Dynamic)
- Thermal
- Fluid Flow
- Hydraulics
- Vibrational analysis
- Geomechanics
- Electro Magnetics
- Bio Medical Engineering
- Nuclear Engineering

The finite element Analysis is used as it possesses a variety of advantages. Few advantages are as listed below

a) Précised Geometrical Representation

b) Analysis of a body with dissimilar material properties

c) Contour representation of the total solution

The Basic principle of the Finite Element Method is to divide the element into finite number of small elements generally of 3 node or 4 nodal elements. Displacement of these nodes is

difficult to find and hence the polynomial interpolation is used to find them. The load/Force is replaced by equivalent system of forces applied at each node. The governing equation used is

$$[F] = [K]\{u\}$$

Where [F] = Force Vector

[K] = Global stiffness matrix

{u} = Nodal displacement

The stiffness matrix [K] depends on the material properties (Isotropic, Orthotropic) and the geometry of the object. The force vector [F] depends on the type of loading and boundary conditions and the direction of the load application. The unknown value {u} can be calculated by mathematical methods internally by the software. The Displacement value is calculated for each of the divided finite element and the average value of the displacement is determined at the nodes. Few steps needed to be followed while modeling and simulation which is clearly explained in [8]. ANSYS 15 workbench is used for finite element modeling and static structural analysis of the package.

5.2 Finite Element Analysis

The basic outline how the finite element analysis problem solving steps is discussed below.

- Geometry
- Material Properties
- Meshing
- Loading and Boundary Condition
- Analysis and Results

The analysis type has been decided based on the type and the method of engineering analysis done. In this study the static structural analysis is used to get the solder joint reliability of the BGA

package. The body with orthotropic properties are directly fed with the appropriate properties in the engineering data sheet.

5.2.1 Geometry

Here in this section the detailed geometry of the body with appropriate dimensions is modeled. The geometric non linearity of be object should be considered before the analysis. Geometric Non linearity s basically classified into two types.

1. Large Deflection and Rotation
2. Stress Stiffening

Non Linearity in the material properties and the orthotropic behavior of the material is one of the critical factor for the Finite element analysis, which indeed has a greater effect on the final solution of the test. If the material exhibits the elastic property up to the proportionality limit in the stress strain curve that means the material doesn't create the stress greater than the yield values. In this case the linear material properties can be used for good approximation. If the material exhibits orthotropic properties and if the deformation was not within the loading condition, then time dependent or temperature dependent material properties needed to be used to get the accurate results. Plastic, creep and viscoelasticity should be considered for such cases. Geometric symmetry can be considered to save the computational time as mentioned in [9]. If the body is symmetric then considering a quarter symmetric model is more advantageous. Once the geometry is model edits always critical to maintain the connectivity between the two bodies and the body needs to be considered as a rigid, friction body etc.

5.2.2 Meshing

Meshing is one of the most critical steps in the FEA. Larger the number of elements results in the better approximation in the solution. Excess number of elements may cause round off error in some of the cases. To avoid this error the meshing should be fine or coarse in appropriate region. Mesh sensitivity analysis can be considered to reduce the computational time while maintaining the accuracy in the solution. Here in this study different methods are used to mesh the model with fine elements while maintaining the connectivity between the elements. Initially the meshing is done with a set of elements and later the number of elements is doubled and compared. If the results are close enough the initial configuration is used to solve the model in order to save the computational time. If the solution are different for both the cases then mesh refinement is done until the results are converged [10]. Different types of elements are used such as 2D and 3D elements based on the application of the analysis.

5.3 Sub Modeling

Basically to get a detailed stress strain contours near the critical parts of the body sub modeling is done. In some cases it may occur that the mesh is too coarse to provide the better results near the critical areas of the object where the stress are higher. Sub modeling is also known as local-global analysis or cut –boundary displacement method. Cut boundary is the method where the critical area is recognized or the part of the body where the stress are higher is determined and the part is sliced from the global model for further analysis. The boundary condition is imported form the global model for the analysis of the sub model. The boundary condition is nothing but the displacement is calculated and is used as the boundary condition in order to maintain the accuracy. The figure 5.1 clearly explains how the sub modeling is done for the area of interest.

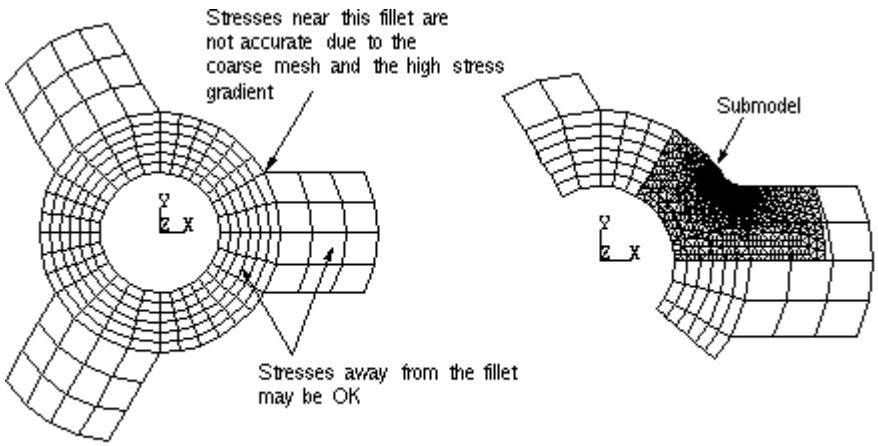

Figure 5.1 Concept of Sub Modeling

The concept of St. Venant's principle explains the sub modeling technique. The Principle states that the actual force distribution is replaced by statically equivalent system, the stress strain distribution is altered only near the region of load application. The principle states that the stress concentration effects are localized near the concentration, i.e., if the boundary condition of the sub model is far away the area of interest accurate and reasonable results can be obtained.

Some of the advantages of sub modeling apart from accuracy in the results are as follows

- Helps in achieving adequate mesh refinement.
- Allows to experiment at different areas of interest
- Decreases the computational time.
- Needed for transition region in solid finite element models is reduced

Chapter 6

FINITE ELEMENT ANALYSIS OF BALL GRID ARRAY PACKAGE

6.1 Modelling Of A Ball Grid Array Package

This chapter discusses the application of FEA modeling and simulation techniques to obtain the fatigue life of the ball grid array package. The basic outline of the design-for-methodology (DFR) is discussed as below.

1. Preprocessing
2. Solving
3. Post processing

Few assumptions are taken to proceed the finite element analysis

- All the parts of the Ball Grid array Package is assumed to be interconnected to each other
- All the components except the solder bump and PCB are assumed to possess linear properties.
- Temperature change in the package during the thermal cycling are assumed to be same throughout the package.

6.2 Geometry

A 3d 11x11 solder bump Ball grid array (BGA) package is modeled using ANSYS v15.0 using the package drawing and X ray images. To validate the dimensions the package is cross sectioned and the dimensions are cross checked and the unavailable dimensions form the drawings are determined. The daisy chain is also attached in the figure 6.3.

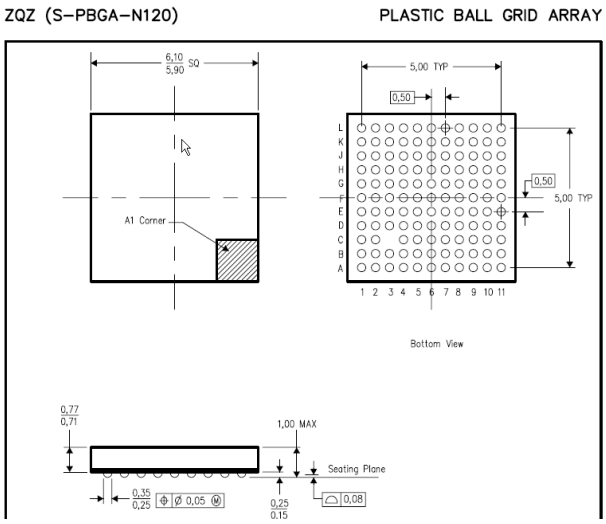

Figure 6.1 Ball Grid Array Package configuration

The basic configuration of the package are obtained from the drawing as shown in the figure 6.1 The pitch of the solder bumps and number of solder bumps are clearly obtained. The standoff height of the package is validate by the microscopic images.

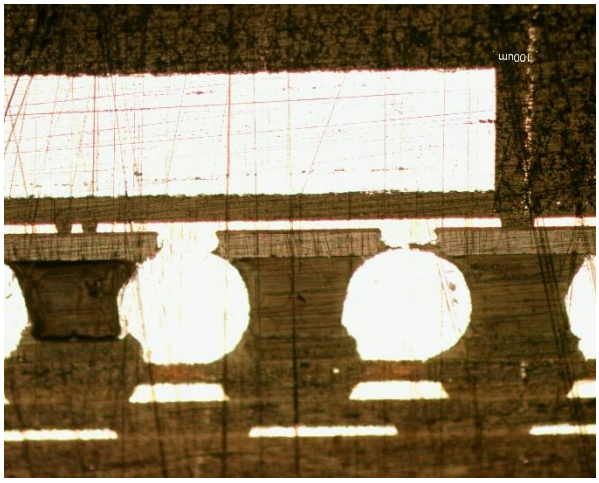

Figure 6.2 Cross section image of the Ball Grid Array Package

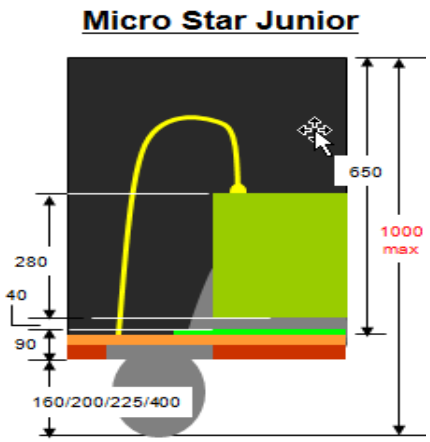

Figure 6.3 Cross section Schematic of the BGA Package

The above image shows the clear picture of the components inside the Ball grid package. The package basically comprise of a copper pad on the top and bottom side of the solder bump. On the Die size the Silicon die is attached which is further attached to polyimide layer with a adhesive layer in the middle. The solder mask in present both on the PCB side and the substrate side as shown in the schematic.

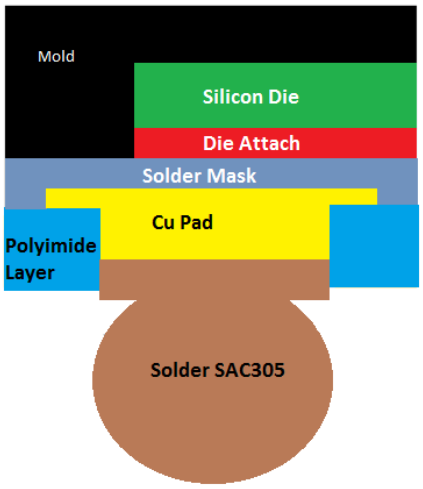

Figure 6.4 Detailed schematic with all the components

The PCB layout is figured out by cross sectioning the PCB as shown in the figure6.5. The detailed PCB with the layers is modeled inside the sub model. The prepreg layer and the number of copper layers inside the PCB is found out and the appropriate dimensions are calculated and a brief schematic with the dimension is made for the clear understanding as shown in the fig6.6. The PCB comprises of 1-6-1 configuration. That is nothing but the PCB comprises of 8 copper layer where ^ copper layers contribute to form the core layer of the PCB and each copper layer on the either side. The prepreg layer is present in between the PCB core layer and the outer most copper layer as shown in the figure 6.6.

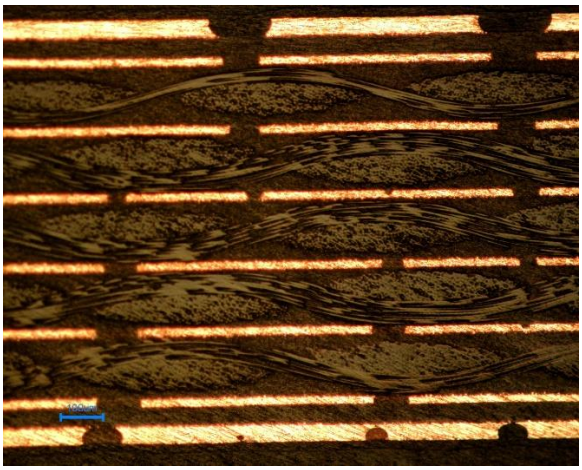

Figure 6.5 Cross section image of the PCB

Figure 6.6 Schematic of PCB layer stack up

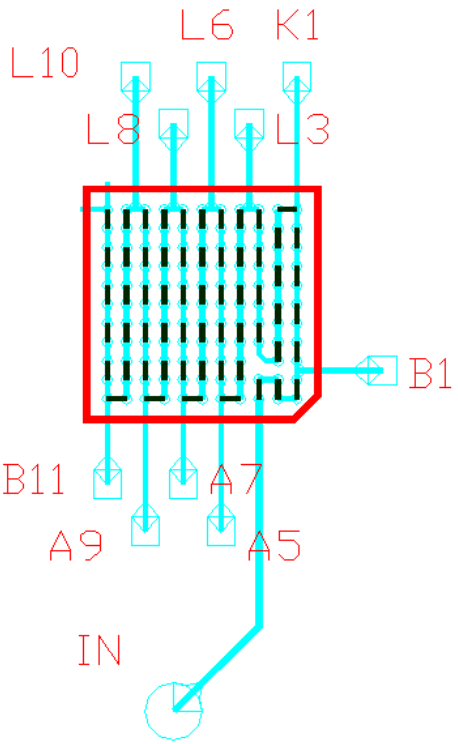

Figure 6.7 Daisy chain of the BGA package

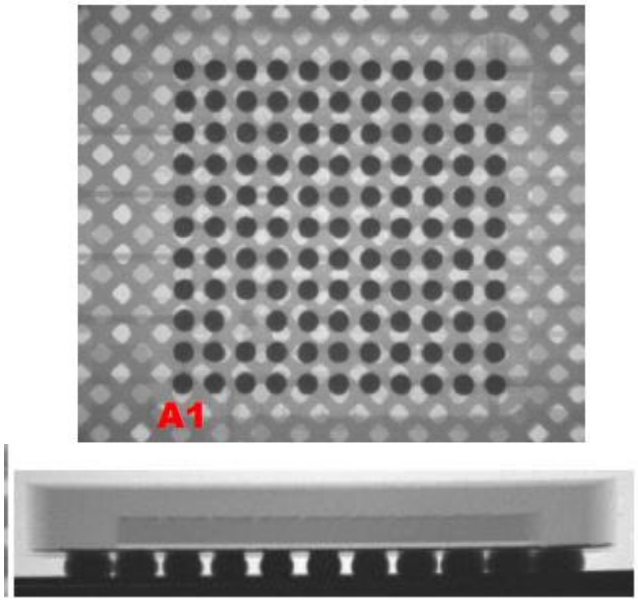

Figure 6.8 x ray image of the BGA Package

The dimension from the drawings, X-Ray images and the cross section images are considered to model a whole 3D model of the Ball Grid Array Package. The FE modeled BGA package is shown in the fig 6.9. Octa symmetric model is modeled for saving the computational time.

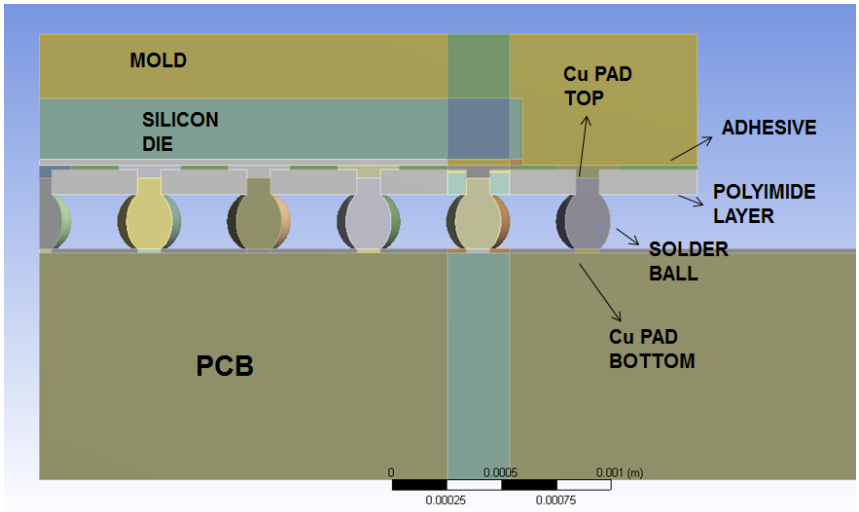

Figure 6.9 FE Model of the Ball Grid Array Package

6.3 Meshing

Different types of elements are used to mesh the model. Hex dominant and three node elements are also used to mesh the model. The Full model is meshed and solved to determine the critical solder joint of the BFA package. Detailed meshing is done in the sub model of the package. A coarse mesh of the BGA package is shown in the figure 6.10. As mentioned earlier an octa symmetric model is used to run the simulation and to determine the critical solder joint. This method is used in order to decrease the computational time while preserving the precision of the results as validated from the literature.

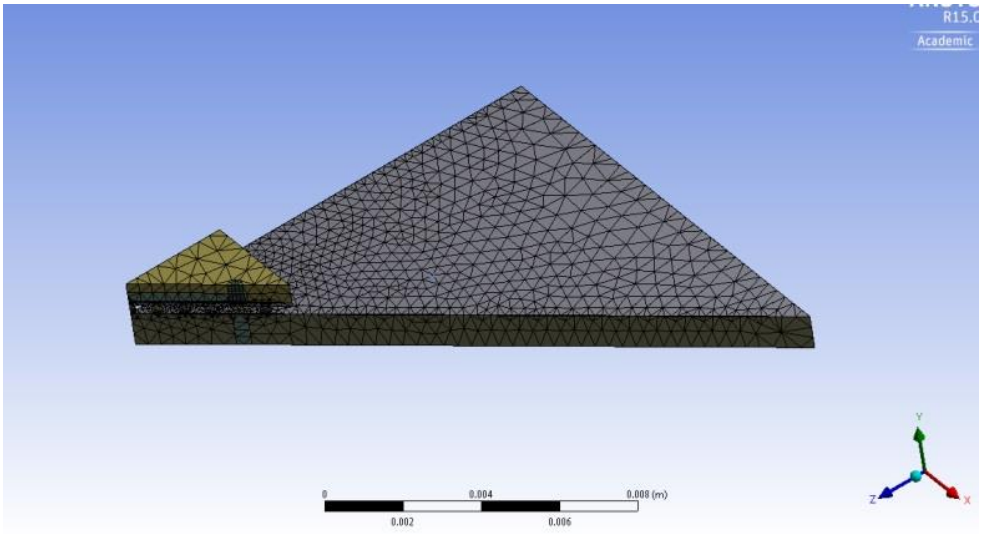

Figure 6.10 Meshed 1/8th model of BGA package

The connectivity between the nodes is maintained to get the appropriate results and stress strain contours. A typical picture showing the connectivity between the elements of the meshed model is shown in the figure 6.11.

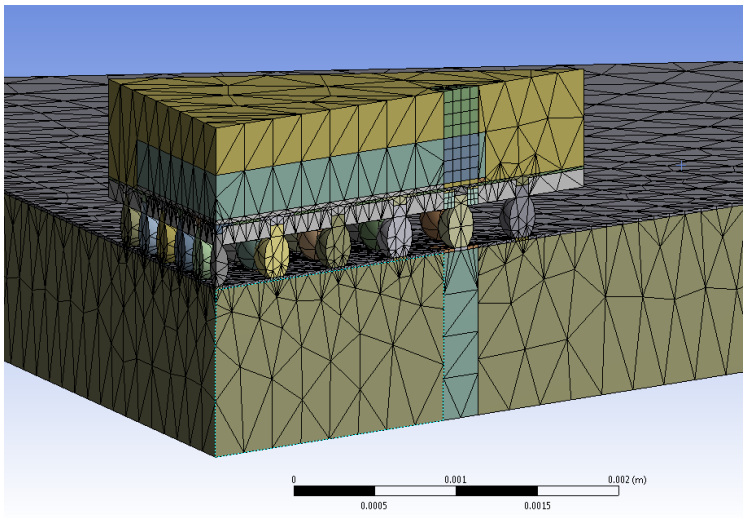

Figure 6.11 Meshed solder balls and other components

6.4 Sub Modelling

Sub modeling is essential whole solving a full 3D model and where the 3D global model is too large to solve or when the loading on the model doesn't have any axes of symmetry. The method of sub modeling employs of capturing the deformation effect on the sub model and using them as the boundary condition while solving the sub model. A coarse global model mesh can be used to capture the effect of 3D deformation and can be transferred to the finer and better meshed sub model to perform the nonlinear detailed strain analysis as mention by Ty et al. [11]. An effective method to analyze the stresses on the solder joints are explained by Yu et al [11].

St. Venant's principle states that if actual distribution of forces is replaced by the statically equivalent system, the distribution of the strain and stress near the regions of load applications are altered. The same principle is used in the sub modeling technique. This implies that the stress concentration affects the localized area around the stress, and if the sub model is far away from the stress concentration accurate results can be obtained. This enables us to achieve more accurate results in the particular region in the model. Sub modeling technique also eliminates the need of transition regions in the solid finite element models.

A 3D octa symmetric model is used with a coarse mesh to identify the critical solder joint i.e., the solder joint with high stress concentration is determined. Extrude tool is used to slice away the critical joint and to prepare a sub model out of it as shown in the figure 6.12. cut boundary interpolations used to transfer the displacement of the sub model form the global model and used as the boundary condition in the local model as shown in the figure 6.13. The nodes of the local model are identified and the software automatically calculates the degrees of freedom (DOF) of each and every node by interpolating the results from the global model. The value obtained are interpolated onto the cut boundary nodes of the sub model using shape functions.

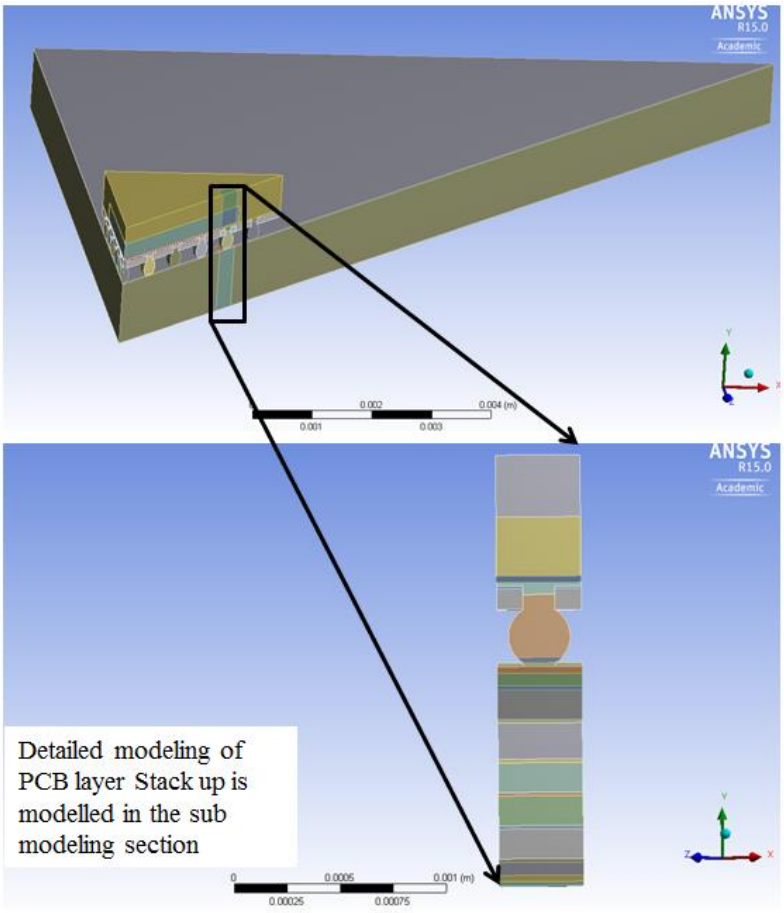

Figure 6.12 PCB layer modelling done in the sub model.

The global model with only a single PCB layer with a solder model on top is used to determine the critical solder bump. For further more analysis to determine the effect of the PCB layer on the solder joint the PCB with the layer stack up is modelled in the sub model for analysis. The sub model with the PCB layers is clearly seen in the figure 6.12. The PCB layers are only modeled in the sub model in order to avoid higher count in the elements while meshing and to decrease the aspect ratio. More the number of elements more is the time taken to solve the model and to avoid the computational time the Layers are modelled only in the sub model.

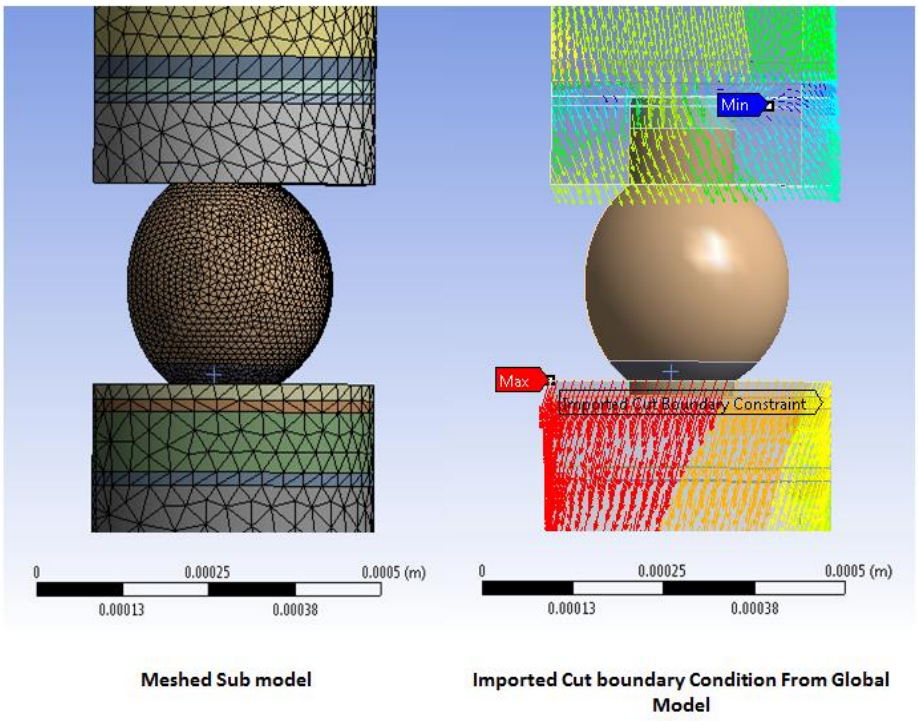

Figure 6.13 Imported cut boundary from the global model

6.5 Material Properties And Boundary Condition

All material properties of the package are considered as the linear elastic material except the solder and FR4 material properties. Orthotropic material properties of the FR4 material is briefly mention in the Table 6.1. Temperature dependent young's modulus, Poisson's ratio and temperature dependent shear modulus are obtained and coefficient of thermal expansion in X, Y and Z directions are given as the input. The linear elastic material properties of all other components are briefly discussed in the Table 6.2.

Table 6.1 Orthotropic Properties of FR4 Material

Young's Modulus (GPa)	Poisson's Ratio	Shear Modulus (GPa)	Coefficient of Thermal Expansion (ppm/°C)
E_x, E_y = 27927-37(T) E_z = 12204-16(T)	ν_{xz}, ν_{yz} =0.39 ν_{xy} = 0.11	G_{xz}, G_{yz} = 5500-7.3(T) G_{xy} = 12600-16.7(T)	α_x,α_y = 1.6e-5 α_z = 8.4e-5

Table 6.2 Material properties of the components of the BGA package

Material	Young's Modulus (Pa)	Poisson's Ratio	Coefficient of Thermal Expansion (ppm/°C)
Die	1.5e 11	0.17	2.9e-6
Die Attach	1.54e 9	0.35	6.5e-5
PCB Soldermask	4.137e 9	0.40	3e-5
Substrate Soldermask	3.5e 9	0.467	5.5e -5
Mold	2.4e10	0.25	8e-6
Adhesive	8.737e 9	0.40	1.46e -5
Polyimide layer	3.3e 9	0.40	3.5e -5

SAC 305 is used to define the material property of the solder ball. Anand's viscoplastic constitutive law is used to describe the behavior of the solder ball. The law states that the dislocation motion of the creep and plastic deformation is combined into the inelastic strain [11].

The total strain is given by the equation

$$\epsilon_{ij} = \varepsilon_{ij}^{e} + \varepsilon_{ij}^{ie}$$

ε_{ij}^{e} *is the elastic strain tensor*

ε_{ij}^{ie} *is the inelastic strain tensor*

Strain rate equation is given by

$$\frac{d\varepsilon_{in}}{dt} = A[\sin h\ (\xi\ \frac{\sigma}{s})]\text{^}(1/m)\ \exp\ (-\frac{Q}{RT})$$

Rate of deformation resistance is given by

$$\acute{S} = \{h_{o}\ (|B|)^{\alpha}\frac{B}{|B|}\}\ \frac{d\varepsilon p}{dt}$$

$$B = 1 - \frac{s}{s*}$$

$$S* = \hat{S}\ [\ \frac{1}{A}\frac{d\varepsilon p}{dt}\ \exp\ (-\ \frac{Q}{RT})]$$

$\frac{d\varepsilon_{in}}{dt}$is the Effective inelastic strain

σ is the effective true stress

S is the deformation resistance

T is the absolute temperature

A is the pre-exponential factor

$\xi$is the stress multiplier

m is the strain rate sensitivity of stress

Q is the activation energy

R is the universal gas constant

$h_o$isthe hardening / softening constant

$\hat{S}$ is the coefficient of deformation resistance saturation value

n is the strain- rate sensitivity

a is the strain-rate sensitivity of hardening/softening.

These material properties are obtained from the industry and the value of the nine Annand's constants is tabulated in the table 6.3. The Poisson's ratio is considered to be 0.4, young's modulus of elasticity E = 194T+100201(MPa) and coefficient of thermal expansion is $0.0022T^2$ + 0.3951T+7.4203 ppm/^oC

Table 6.3 Anand'sVisco Elastic Properties of SAC 305

ANAND'S CONSTANTS	Value
Initial value of deformation resistance (MPa)	1800x(6.894757e-03)
Activation energy/universal gas constant (1/K)	9400
Pre-exponential factor (1/sec)	4.0e+06
Stress multiplier	1.5
Strain rate sensitivity of stress	0.303
Hardening/softening constant (MPa)	2.0e+05x(6.894757e-03)
Coefficient of deformation resistance (MPa)	2.0e+05x(6.894757e-03)
Deformation resistance value	0.07
Strain rate sensitivity of hardening or softening	1.3

The Boundary imposed on the global model is shown in the figure 6.12. Since the octa symmetric model in used the faces are applied with symmetry boundary condition. The center node is fixed i.e., $U_z = 0$, to prevent rigid body motion.

The thermal condition used for the simulation is the same thermal condition used to obtain the BLR data. The temperature profile used is shown in the figure 6.14. The simulation is run for over compete three cycles to obtain a stable stress-strain hysteresis loop. The initial stress free temperature is set to the room temperature i.e., 25ºC.

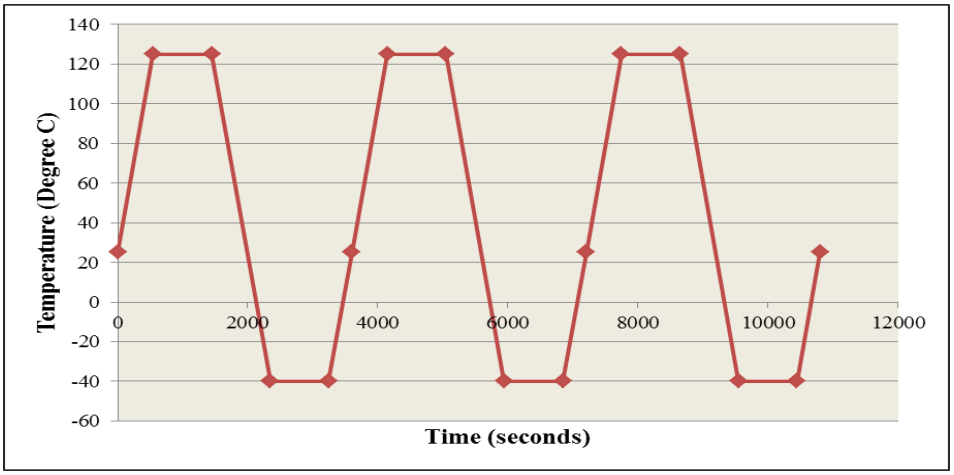

Figure 6.14 Temperature profile

Chapter 7

FATIGUE LIFE PREDICTION MODELS

7.1 Introduction

The fatigue life models are basically used to predict the life of the packages. Generally the solder joints subjected to thermal cycling tend to fail in the low cycle fatigue (LCF) due to the thermos mechanical failure. The fatigue damage parameters include the creep strain range, plastic strain range and inelastic strain energy density. The fatigue life generally falls between 100 to 10,000 thermal cycles. Here in this study the cycles to failure are calculated from the BLR data and the inelastic strain energy density is calculated which have a good correlation index to the BLR data [12][13][14]. The Volume average strain energy density is used further by fatigue life prediction models to calculate the fatigue life and in compared with the experimental data.

The energy based fatigue model employs the cyclic stress – strain hysteresis loop to compare the inelastic dissipated energy (plastic work) and the elastic strain energy density [11].

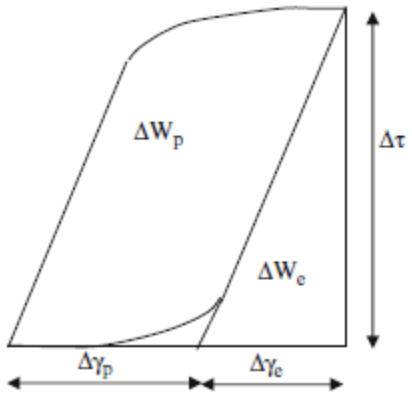

Figure 7.1 Cyclic Stress- Strain Hysteresis loop

In this study the energy based fatigue models are used to predict the characteristic life of the package and compared with the experimental BLR data. The Energy based models used are discussed below

7.2 Energy Based Models

Darveaux [12] stated that the increase in the inelastic strain energy density per cycle can be considered as the fatigue indicator for the package. The inelastic strain energy density is mathematically given by the formula

$$W^{in} = \int \sigma_{ij} d\varepsilon_{ij}^{in}$$

Where σ_{ij} is the Stress tensor

ε_{ij}^{in} is the inelastic strain tensor

Schubert [14] established a fatigue model based on the dissipated energy density during one thermal cycle and the characteristic life. The proposed model is applicable for ball grid array and chip scale packages as well. The solder alloys used are SnPbAb and SnAgCu solder alloys as shown in figure [7.2]. The SAC solder is used in the present work and the equation to calculate the characteristic life is given by

$$N_f = 345 W_{cr}^{(-1.02)}$$

Where N_f is the characteristic life (cycles to 63.2% Failures)

W_{cr} is the calculated strain energy density per cycle.

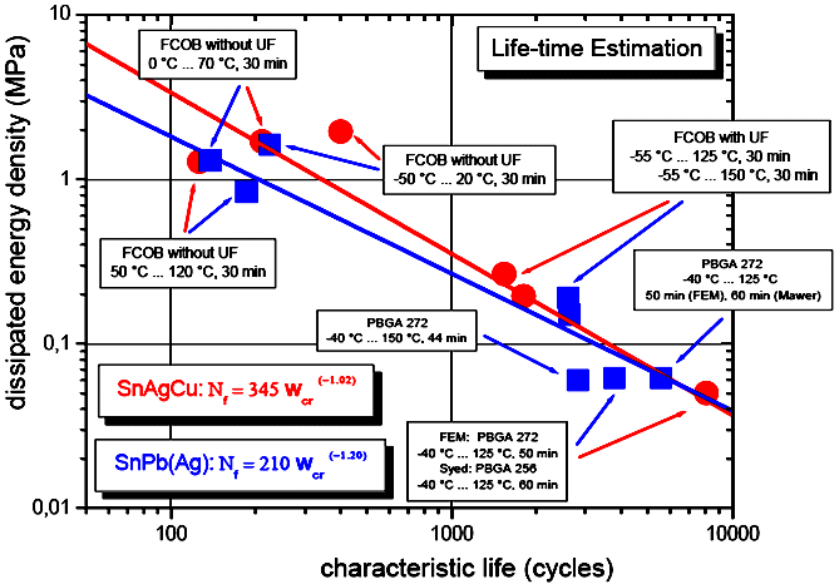

Figure 7.2 Schubert's Energy based model for SAC and SnPb Solder

Morrow's energy based model is also used to predict the low cycle fatigue life Nf from the inelastic strain energy density Wp (MPa) [15]. The equation to predict the low thermal fatigue life is given by

$$N_f^n W_p = A$$

Where A is the material ductility coefficient

n is the fatigue exponent

The value of A (Material ductility) is determined for SnAgCu solder alloys by Pang [16] which will be further used in this study to determine the life of the package.

Syed [17] used a SnAgCu solder material for life prediction of CSP and BGA packages using the strain energy density. The inelastic strain energy density is also called as the accumulated plastic work. The equation proposed by syed is as follows

$$Nf = 674.08\ (\Delta W)^{(-0.9229)}$$

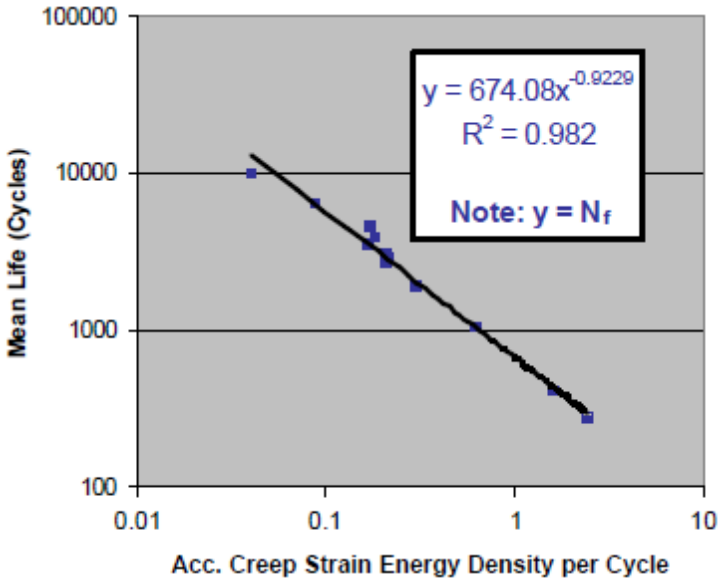

Figure 7.3 Syed's Energy based model for CSP and BGA Packages.

Chapter 8

RESULTS AND DISCUSSION

The basic aim of this study is to determine the characteristic life of the package using the various fatigue life prediction models. The energy based fatigue models are used to calculate the life of the package for which the inelastic strain energy density, also known as the plastic work is used. The Volume averaging technique is implemented in order to calculate the strain energy density. The Critical solder joint is determined from the static structural analysis under thermal loading and a 25 microns tick portion from the critical part is considered for the volume averaging process. The stress free temperature is set to the room temperature during the simulation for all the cases. Three complete cycles are considered to obtain a stable stress – strain hysteresis loop. The choice is anyways dependent on the computational time and the stabilization of the system as mentioned in [19].

As the element size in the solder joint decreases, the calculated strain energy increases. And hence the volume averaging technique is leveraged and to reduce the mesh sensitivity. The strain energy of each element is normalized by the volume of the element.

$$\Delta W_{avg} = \frac{\Sigma \Delta W \, x \, V}{\Sigma V}$$

Where ΔW_{avg} is the accumulated viscoplastic strain energy density per cycle

ΔW is the accumulated viscoplastic strain energy density for each element per Cycle.

V is the volume of each element

The simulation in interpolated for each and every element select in the 25 micron thick portion form the critical solder joint. The fatigue life indicator ΔW is calculated from the difference of ΔW_{avg} from the third and second cycle.

$$\Delta W = (\Delta W_{avg})\ 3^{rd} - (\Delta W_{avg})\ 2^{nd}$$

The characteristic life of the solder joint is calculated for the Ball grid array package and is compared with the experimental BLR data. The accumulated volume averaging plastic work is calculated for the temperature cycle used for the experimental data. A typical Weibull plot foe the BGA package under specified thermal condition is shown in the figure 8.1.

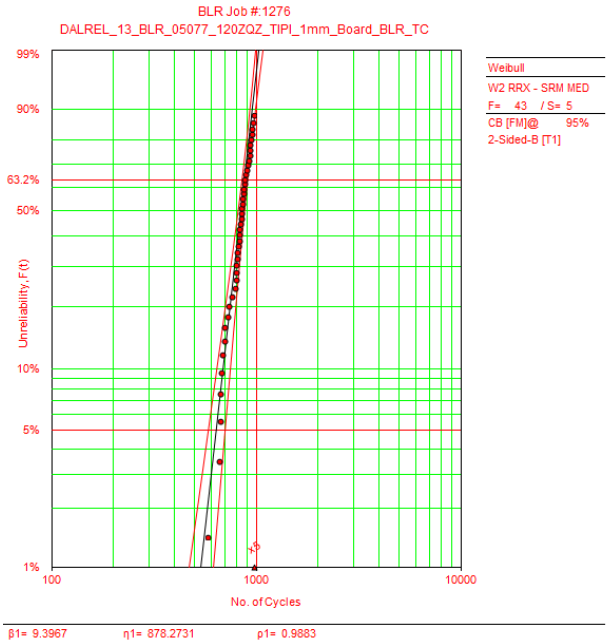

Figure 8.1 Weibill plot for the BGA package under Thermal condition.

The calculated strain energy density is. Substituted in the equations proposed by various fatigue life prediction models. Schubert's Morrow's and Syed's model is used to predict the life. The table 8.1 shows the comparative study of various life prediction models with experimental BLR data. And a chart is plotted as shown in the figure 8.2 to determine the lease %error in the prediction model.

Table 8.1 BLR data and Prediction model comparison table

Model	Characteristic Life N_f Cycles to 63.2% failure	Total Percentage	Percentage difference
BLR Data	577.00	100.00	0.00
Morrow's Model	461.63	80.00	20.00
Syed's Model	840.57	145.68	-45.68
Schubert's model	270.32	46.85	53.15

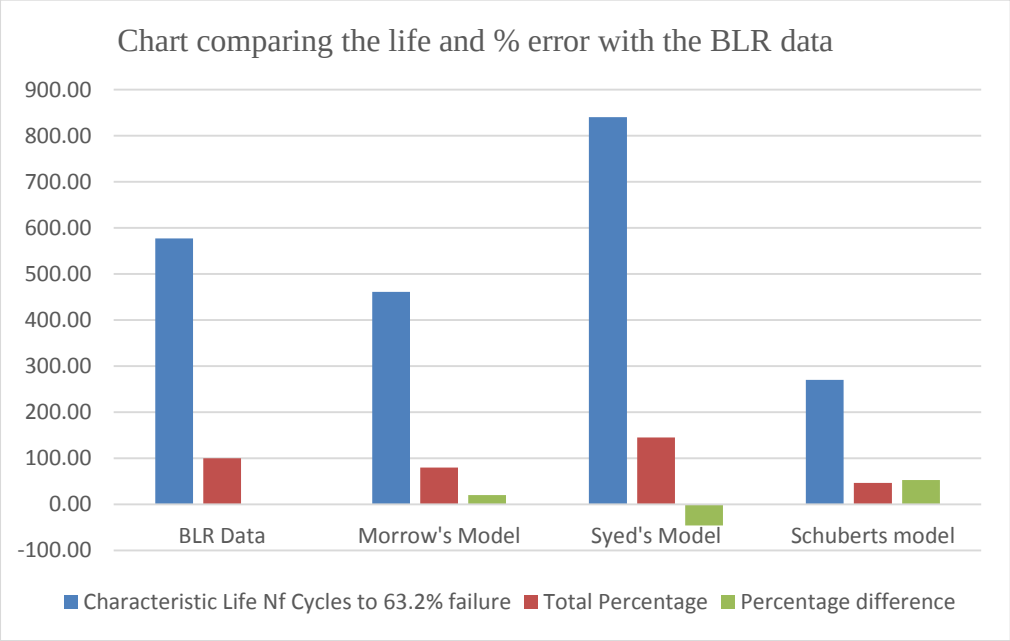

Figure 8.2 Chart comparing the % Error with the BLR data

It is found out that the Morrow's model has the least % error with the BLR data about 5% which is taken for further analysis by changing the PCB parameters and predicting the life for each case. Here four cases are considered for further analysis. Few changes in the dimensions in the copper layer thickness are made to check the reliability of the package. The Stiffness of the Prepreg is also change for furthermore analysis. The four different cases we work on are as follows.

- PCB with 50% Increased copper thickness in the outermost layer.
- PCB with 50% Decreased copper thickness in the outermost layer.
- PCB with 50% Increased Prepreg stiffness in the outermost layer.
- PCB with 50% Decreased Prepreg stiffness in the outermost layer.

The Volume average plastic work is calculated for all the four cases and the three fatigue life prediction models as mentioned earlier are used to get the characteristic life for each case. A comparison chart for all the cases with the fatigue life calculated using the three models are shown in the table 8.2.

Table 8.2 Fatigue life comparison table for all the cases

cases	Schubert's model	Morrow's Model	Syed's Model
PCB with all Layers	270.32	461.63	840.57
PCB with 50% increase in cu thickness	385.65	680.70	609.46
PCB with 50% decrease in cu thickness	308.18	532.74	746.55
PCB with 50% increase in prepreg stiffness	269.72	460.51	842.25
PCB with 50% decrease in prepreg stiffness	508.74	921.40	474.34

The morrow's model has the low % error and hence the Morrow's model to predict the fatigue life is standardized for further analysis in the study. The volume averaging accumulated elastic strain energy density is calculated for the PCB with the outer most copper thickness increased by 50% and decreased by 50% and is shown in the figure 8.3. Less the plastic work calculated more is the life of the package. It is calculated and is found out to be that the PCB ith50% increase in the copper content in the outer most layer has the lower elastic strain energy density than the other case. By increasing the copper by 50% the reduction in the accumulated plastic work is observed to decrease by 30% as shown in the figure below.

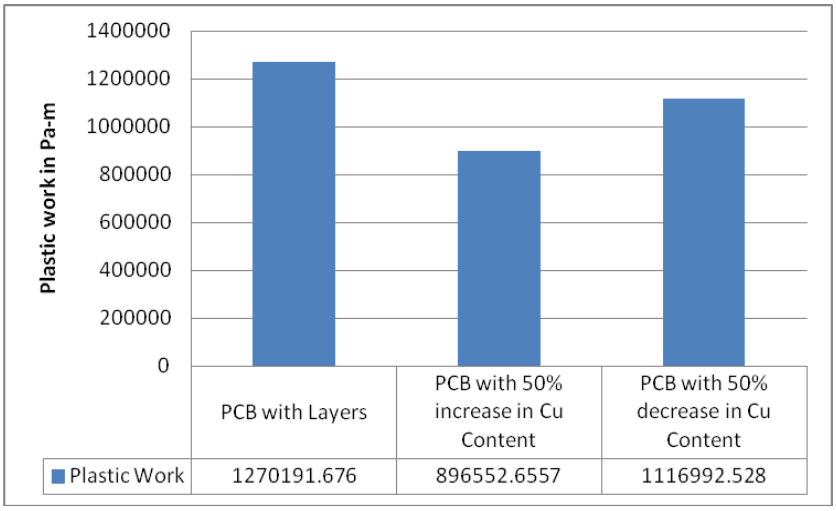

Figure 8.3 Plastic work comparison chart for the change in copper thickness

Equivalent plastic strain for the critical solder ball is calculated for the better understanding. The maximum Equivalent plastic strain in the critical solder ball is considered and a comparison chart for with change in the copper thickness in shown in the fig 8.4. The figures 8.5 and 8.6 shows the equivalent plastic strain distribution in the solder joint with increase in copper thickness in the outer most layer by 50% and decrease by 50% respectively.

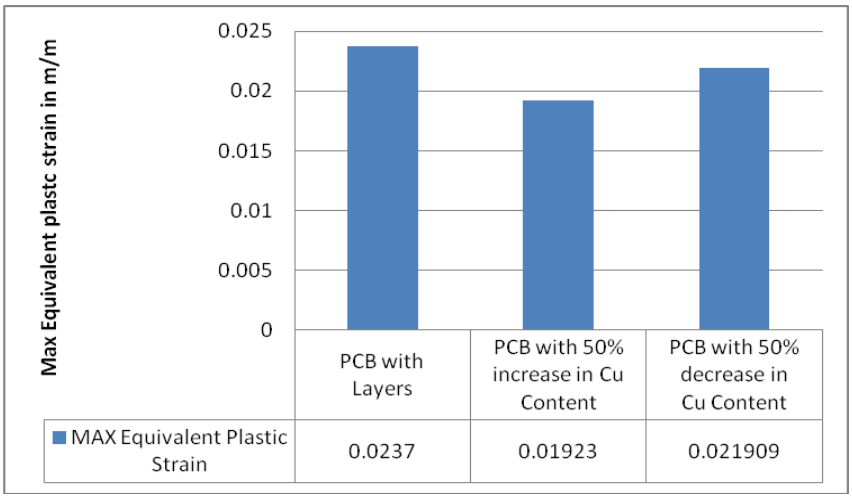

Figure 8.4 Maximum equivalent plastic strain comparison chart for the change in copper thickness

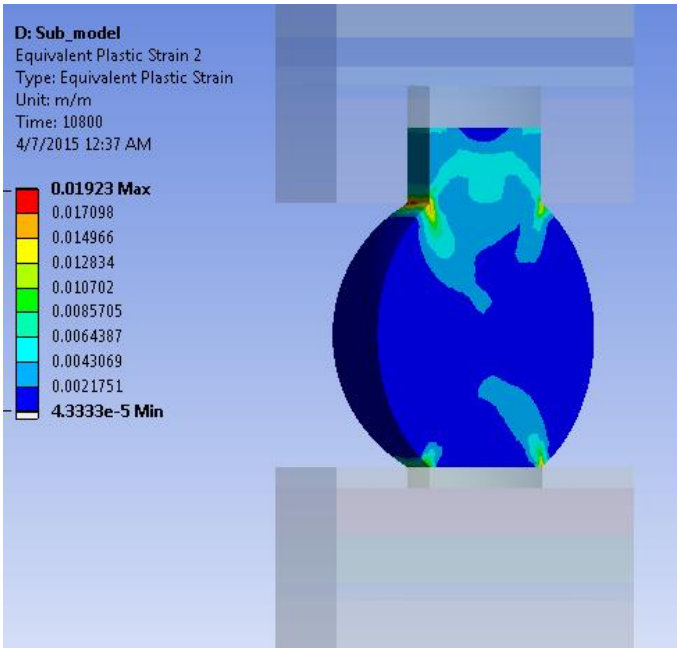

Figure 8.5 Equivalent plastic strain Distribution for the critical solder ball with 50% increase in copper thickness

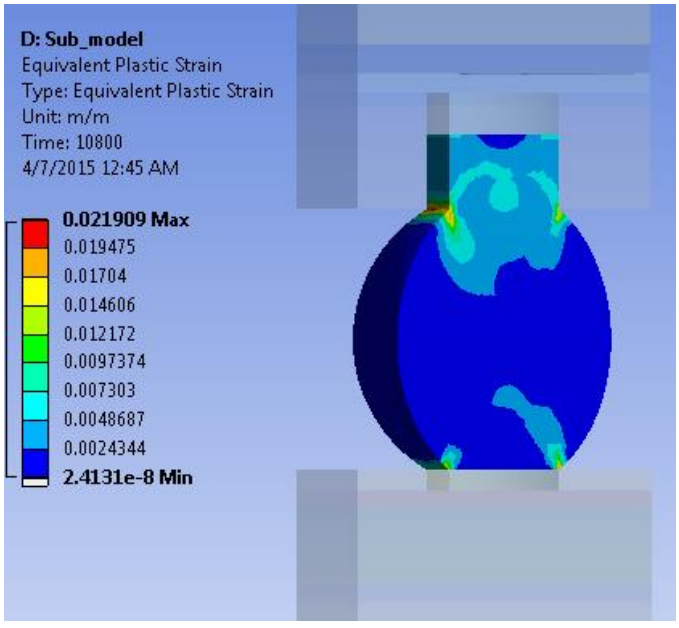

Figure 8.6 Equivalent plastic strain Distribution for the critical solder ball with 50% decrease in copper thickness

The same analysis is done for the change in the prepreg stiffness with increment and decrement by 50% while the copper thickness in unaltered. The copper thickness is kept as it was before and the prepreg material stiffness in altered and the analysis is done. It is observed that the prepreg with 50% decrease in the stiffness caused the accumulated plastic work to decrease by 50% which is very significant. A Graph showing the comparison inelastic work with change in the Prepreg parameters is shown in the figure 8.7. For a better understanding a comparison is done for the maximum equivalent plastic strain for the critical solder joint for the change in prepreg stiffness is shown in the fig 8.8. The equivalent plastic strain distribution is presented in the figures 8.9 and 8.10 respectively.

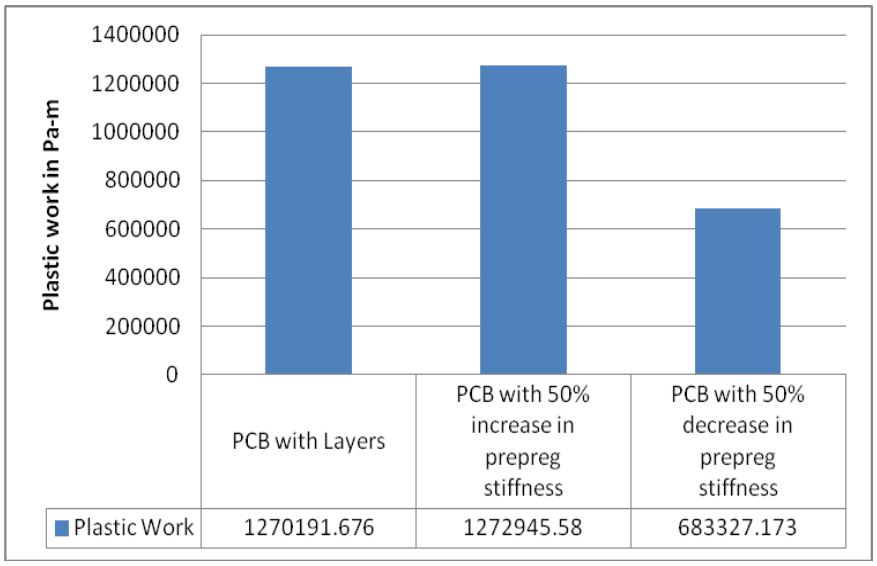

Figure 8.7 Plastic work comparison chart for the change in Prepreg Stiffness

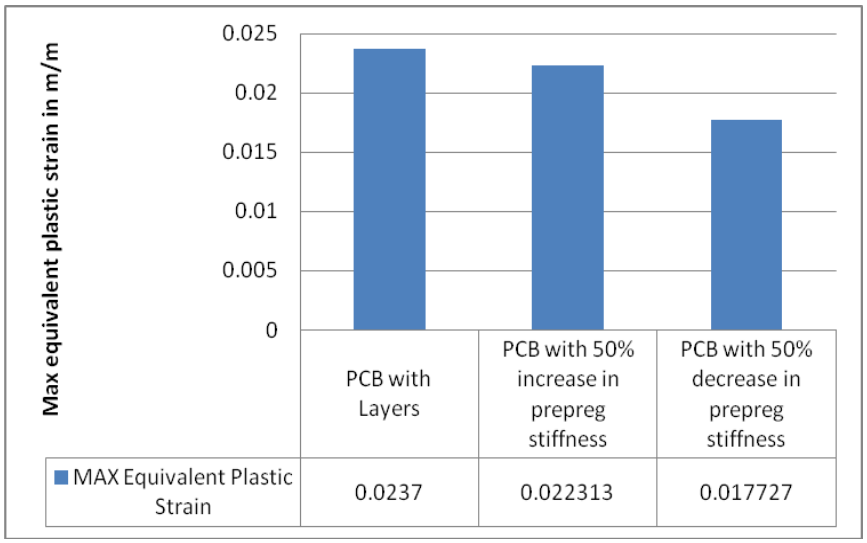

Figure 8.8 Maximum equivalent plastic strain comparison chart for the change in Prepreg stiffness

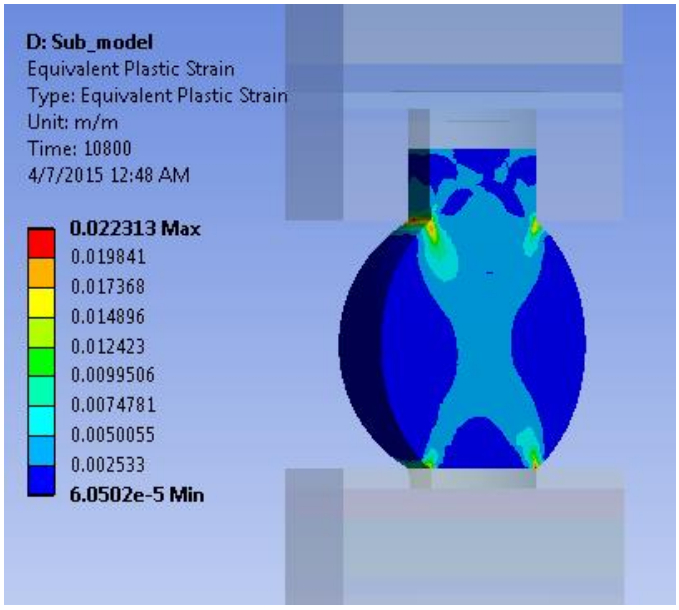

Figure 8.9 Equivalent plastic strain Distribution for the critical solder ball with 50% increase in Prepreg stiffness

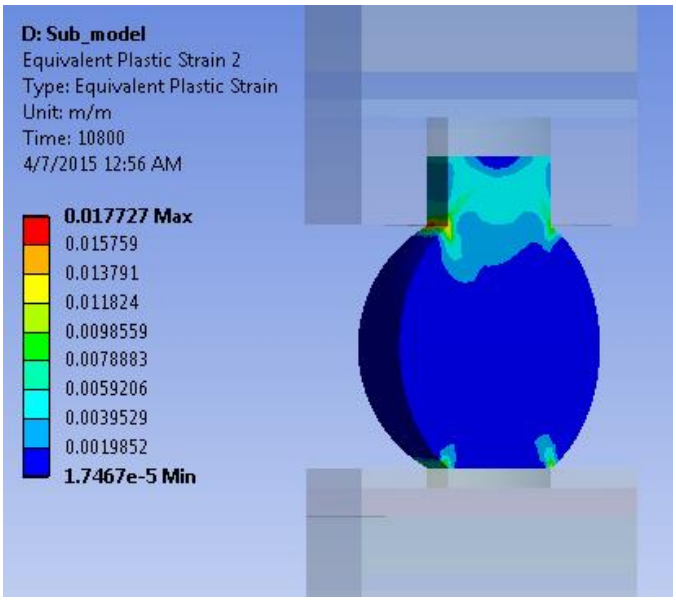

Figure 8.10 Equivalent plastic strain Distribution for the critical solder ball with 50% decrease in Prepreg stiffness

After conducting various simulations and experiments it can be concluded that the prediction model depend on the package family and the solder alloy used. Form the data obtained and the analysis conducted it is seen that the copper thickness increase by 50% in the outer most layer increases the life of the BGA package by 30%. It is also observed that by decreasing the prepreg stiffness by 50% also increased the characteristic life of the package by 50%.

APPENDIX

APDL SCRIPT USED FOR STRAIN ENERGY DENSITY

```
!   Commands inserted into this file will be executed immediately after the
ANSYS /POST1 command.

!   Active UNIT system in Workbench when this object was created:  Metric (m,
kg, N, s, V, A)
!   NOTE:  Any data that requires units (such as mass) is assumed to be in the
consistent solver unit system.
!               See Solving Units in the help system for more information.


!APDL SCRIPT TO CALCULATE PLASTIC WORK
/post1
allsel,all
!CALC AVG PLASTIC WORK FOR CYCLE1
set,5,last,1 !LOAD STEP
cmsel,s,botsolder,elem !ELEMENT FOR VOL AVERGAING
etable,vo1table,volu
pretab,vo1table
etable,vse1table,nl,plwk !PLASTIC WORK
pretab,vse1table
smult,pw1table,vo1table,vse1table
ssum
*get,splwk,ssum,,item,pw1table
*get,svolu,ssum,,item,vo1table
pw1=splwk/svolu !AVERAGE PLASTIC WORK
!CALC AVG PLASTIC WORK FOR CYCLE2
set,10,last,1 !LOAD STEP
cmsel,s,botsolder,elem
etable,vo2table,volu
pretab,vo2table
etable,vse2table,nl,plwk !PLASTIC WORK
pretab,vse2table
smult,pw2table,vo2table,vse2table
ssum
*get,splwk,ssum,,item,pw2table
*get,svolu,ssum,,item,vo2table
pw2=splwk/svolu !AVERAGE PLASTIC WORK
!CALC DELTA AVG PLASTIC WORK
pwa=pw2-pw1
!CALC AVG PLASTIC WORK FOR CYCLE3
```

```
set,15,last,1 !LOAD STEP
cmsel,s,botsolder,elem
etable,vo3table,volu
pretab,vo3table
etable,vse3table,nl,plwk !PLASTIC WORK
pretab,vse3table
smult,pw3table,vo3table,vse3table
ssum
*get,splwk,ssum,,item,pw3table
*get,svolu,ssum,,item,vo3table
pw3=splwk/svolu !AVERAGE PLASTIC WORK
!CALC DELTA AVG PLASTIC WORK
pwb=pw3-pw2
```

REFERENCES

[1]. D. R. Frear, L. N. Ramanathan “Emerging Reliability Challenges in Electronic Packaging” J.-

[2]. RavikumarSanapala ”Characterization of fr-4 printedcircuit board laminates beforeand after exposure to lead-freesoldering conditions”

[3]. Lau, John H., "Effects of Build-up Printed Circuit Board Thickness on the Solder Joint Reliability of a Wafer Level Chip Scale Package (WLCSP)",

[4]. Primavera, Anthony. A., "The influence of PCB parameters on CSP assembly and reliability".

[5]. BijuChandrana , Deepak Goyalb& Jeffrey Thomas “Effect of Package Design and Layout on BGA Solder Joint Reliability of an Organic C4 Package”

[6]. Pardeep K. Bhatti1 , Min Pei2 , and Xuejun Fan “Reliability Analysis of SnPb and SnAgCu Solder Joints in FC-BGA Packages with Thermal Enabling Preload”

[7]. Rommel Cintró and Mayagüez Dr. Victor Saouma “Strain Measurements with the Digital Image Correlation System Vic-2D”

[8]. T. Raman, "Assessment of The Mechanical Integrity of CU/LOW-K Dielectric In A Flip Chip Package," Master's Thesis, UT Arlington, Arlington, 2012.

[9]. E. Madenci, *The Finite Element Method and Applications in Engineering Using ANSYS*, XVI ed. Springer, 2007.

[10]. "Introduction to ANSYS Meshing” Lecture 3, 15.0 Release.

[11]. J. Pang, *Lead Free Solder: Mechanics and Reliability*, X ed. Springer, 2012.

[12]. R. Darveaux, "Effect of simulation methodology on solder joint crack growth correlation," in *ECTC*, Las Vegas, 2000.

[13]. L. F. Coffin, "A study of the effects of cyclic thermal stresses on a ductile metal," ASME, 1954. S. S. Manson, "Fatigue: a complex subject-some simple approximation,"

[14]. A. Schubert, R. Dudek, and E. Auerswald, "Fatigue life models for SnAgCu and SnPb solder joints evaluated by experiments and simulation," in *ECTC*, New Orleans, 2003, pp. 603-610.

[15]. J. D. Morrow, "Cyclic plastic strain energy and fatigue of metals," American Society for Testing and Materials Testing Standard ASTM STP 378, 1964.

[16]. J. H. Pang, B. S. Xiong, and T. H. Low, "Creep and fatigue characterization of lead free 95.5Sn-3.8Ag-0.7Cu solder," in *ECTC*, 2004, pp. 1333-1337Vol2

[17]. A. Syed, "Accumulated creep strain and energy density based thermal fatigue life prediction models for SnAgCu solder joints," in *ECTC*, 2004, pp. 737-746Vol1.

[18]. X. Fan, M. Pei, and P. K. Bhatti, "Effect of finite element modeling techniques on solder joint fatigue life prediction of flip-chip BGA packages," in *ECTC*, San Diego, 2006.

[19]. X. Fan, M. Pei, and P. K. Bhatti, "Effect of finite element modeling techniques on solder joint fatigue life prediction of flip-chip BGA packages,"

[20]. Mguil-Touchal, F. Morestin, M. Brunet."Various experimental applications of digital image correlation methods".

[21]. Rommel CintrÛn ,Dr. Victor Saouma "Strain Measurements with the Digital Image Correlation System Vic-2D"

[22]. Po-Chih Hung and A. S. Voloshin "In-plane Strain Measurement by Digital Image Correlation"

[23]. Stephen Hall "Full-field displacement/strain measurements and Digital Image Correlation principles and methods"

.

BIOGRAPHICAL INFORMATION

Sanjay MahesanRevathi received his bachelor's degree in Aeronautical engineering From Jawaharlal Nehru Technological University in the Year 2012. He pursued his masters in mechanical engineering in the University of Texas at Arlington in fall 2013. He was an acting member in the Electronic MEMS &Nano electronics Systems Packaging Centre (EMNSPC) from his first semester. He was a research assistant under the supervising professor Dr. DerejeAgonafer and was into reliability team with keen interest in the failure analysis of the electronic packages. His research mainly included the Experimental material characterization of the PCB, fracture mechanics and thermos-mechanical simulation of the electronic packages. He was also a part of the research team, and a integral part of the SRC funded project where he worked closely with industrial liaisons. After graduation Sanjay plans to pursue his further career in the field of electronic packaging and semiconductor industries.